Master thesis : Cubesat deployment

Auteur : Duijsens, Sébastien
Promoteur(s) : Bruls, Olivier
Faculté : Faculté des Sciences appliquées
Diplôme : Master en ingénieur civil en aérospatiale, à finalité spécialisée en "aerospace engineering"
Année académique : 2016-2017
URI/URL : http://hdl.handle.net/2268.2/2586

Université de Liège

Faculty of Applied Sciences

Preliminary study of a deployable CubeSat

Author:
Sébastien Duijsens

Supervisors:
Olivier Brüls
Jean-Yves Plesseria

Readers:
Jean-Claude Golinval
Gaëtan Kerschen

Graduation Studies conducted for obtaining the Master's degree in Aerospace Engineering

Academic year 2016-2017

Abstract

This paper is about the feasibility study of a deployable Earth observation small satellite. The satellite is a 6U CubeSat carrying two telescopes that have to be deployed with a very high accuracy in order to improve the resolution of the images by interferometry. A review of deployable structure for satellites is done to determine the most appropriate deployment mechanism, the one that corresponds to the most accurate deployment and the most rigid deployed structure.

Then, a preliminary design is made, followed by a modal study of the deployed structure and by a thermal analysis of the spacecraft. Finally, it is assessed that the satellite respects the CubeSat requirements. So a mass and power budget are done, with an evaluation of the center of gravity of the spacecraft.

Contents

List of Figures

List of Tables

List of Abbreviations and Acronyms

ADCS	Attitude Determination and Control System
CAD	Computer Aided Design
CFRP	Carbon Fiber Reinforced Polymere
CTM	Collapsible Tube Mast
DS	Deep Space
ELF	Extremely Low Frequency
EMC	Elastic Memory Composite
EPS	Electric Power System
ESA	European Space Agency
GMI RDA	GPM Microwave Imager Reflector Deployment Assembly
ISARA	Integrated Solar Array and Reflectarray Antenna
ISIS	Innovative Solutions In Space
ISS	International Space Station
IXO	International X-ray Observatory
JAXA	Japan Aerospace Exploration Agency
JPL	Jet Propulsion Laboratory
LEO	Low Earth Orbit
MAC	Multiple Alkylated Cyclopentanes
MAOT	Multiple Aperture Optical Telescope
MLI	Multi-layer Insulation
MPACS	Micro-Propulsion Attitude Control System
NASA	National Aeronautics and Space Administration
NuSTAR	Nuclear Spectroscopic Telescope Array
P-POD	Poly-Picosatellite Orbital Deployer
PFPE	Perfluoropolyethers
PRISM	Pico-satellite for Remote-sensing and Innovative Space Missions
PTFE	Polytetrafluoroethylene
SIM	Space Interferometry Mission
STEM	Storable Tubular Extendible Member
TRAC	Triangular Rollable and Collapsible
UK ATC	UK Astronomy Technology Centre
USAFA	United States Air Force Academy
VLT	Very Large Telescope

Acknowledgements

First, I am grateful to the Centre Spatial de Liège for giving me the opportunity to make my internship in such a great place.

Then, I would like to thank more specifically my supervisors in the Centre Spatial de Liège, Jean-Yves Plesseria and Lucas Salvador, for their support throughout this work and the time they took for me.

Furthermore, I would like to thank my supervisor at the Université de Liège, Prof. Olivier Brüls for his availability and his advice.

Finally, I am grateful for all the other people that helped me for this work and in particular Jérome Loicq for its guidance for the optical part.

1 Introduction

These last years, a new category of spacecraft has emerged: the miniaturized satellites. These small satellites present many advantages, particularly their attractive low cost and development time which are combined with decent performances, making them often technology testers. Nowadays, the electronics miniaturization and the technological progress enable the smallsats to perform more tasks with a lower cost.

However, the small payload is also the bottleneck of the CubeSat industry. Indeed, for the satellites dedicated to observations, the optical aperture size is limited, as well as the resolution, and the signal-to-noise ratio. Moreover, observations in some frequency range need a focal length of at least 2m.

Therefore, there are solutions to improve the quality of observations. Interferometry can be used in this goal, either with several independent satellites combining their measurements to a central spacecraft. Or by using deployable structures.

Deployable structures have a long history in the space industry, and have been used for years to deploy solar panels or antennas, among other things. Several techniques have been studied and tested on missions, each of them presenting benefits and disadvantages.

The objective of this work is to study the feasibility of a deployable CubeSat carrying two telescopes which collect light that is combined by interferometry on a central detector. These instruments have to be taken away using a reliable and accurate deployment technique, and the deployed structure has also to be the most rigid as possible.

First, a review of all the deployable structures existing is conducted. They are classified according to their category and the deployment technique used, in order to select the most suitable for this work. Then, a preliminary design of the CubeSat is made, with all the components on-board including the deployable structure. After that, a modal analysis is carried out with the software *Samcef*, to evaluate the rigidity of the deployed satellite. The mode shapes of the structure is studied, as well as its response to an external acceleration.

Another section is dedicated to a thermal analysis, made with the objective to determine, in different situations, the elongation of the deployed structure.

Finally, the last section assesses the feasibility of the study, identifies areas for improvement and points what could be done in the future.

2 Context of the mission

First of all, it is important to start with an historical background about CubeSats and deployable structures for large and small satellites. This will help to make the right choices for this study, in particular to select the most appropriate deployment technique.

2.1 About CubeSats

The CubeSat Project began in 1999 from a collaboration between two universities, California Polytechnic State University and Stanford University, and had the goal to provide standard specifications for small satellites. In the beginning, a CubeSat was defined as a 10 cm cube with a mass of 1kg, which corresponds to one unit (1U). The primary mission of the CubeSat Program was to facilitate access to space for small payloads and to reduce cost and development time by imposing a standard design. Then specifications have changed over time and nowadays there are plenty of CubeSats bigger than 1U with the following main features :

- 1U is a 10cm x 10cm x 11.35 cm cube with a mass up to 1.33 kg, [1]
- 2U is a 10cm x 10cm x 22.7 cm cube with a mass up to 2.66 kg,
- 3U is a 10cm x 10cm x 34.05 cm cube with a mass up to 4 kg,
- 6U is a 10cm x 22.63cm x 36.6cm cube with a mass up to 12 kg. [2]

This list is not exhaustive, and by now it is possible to build even bigger CubeSats : 8U, 12U or 16U. Due to their small size, CubeSats are generally launched as a secondary payload. So a standardization of their design makes their insertion inside launchers easier, as well as their deployment in orbit.

During launch, they are stacked inside a standard deployment system that holds up to three CubeSats and eject them after reaching orbital altitude. These systems are called dispenser and serve as interface between the launch vehicle and CubeSats. Originally, there was only the Poly Picosatellite Orbital Deployer used, which can contain up to three CubeSats 1U, or a single 3U, but is not compatible with bigger satellites. Fortunately, multiple companies like ISIS or Tyvak are developing 6U dispensers which are represented in Figure 1. [3]

(a) P-POD (b) Isis (left) and Tyvak (right) dispensers

Figure 1: Different types of dispensers

Actually, CubeSats are just a subcategory of the small satellites class, which comprises any satellite below 500kg, heavier spacecraft are categorized as large satellites. And inside this category satellites are again classified according to their mass, with CubeSats situated between microsatellites and nanosatellites.

Category	Mass range [kg]
Minisatellites	100 - 500
Microsatellites	10 - 100
Nanosatellites	1 - 10
Picosatellites	0.1 - 1
Femtosatellites	< 0.1

Table 1: Small satellites classification

The standardized CubeSat Satellite platform has also allowed new actors such as small companies and universities to take part of the space field. Indeed, the low cost of production of this kind of satellite has a lot of interests for them. For the students, it has an educational interest because it enables them to work on real projects. It is also an inexpensive means to engage them in all phases of satellite development, operation and exploitation through hands-on research and development experience.

Space companies have also interests in that business, because they can get good results with a low investment. Moreover it can be a way to test new technologies or to verify the feasibility of a bigger mission at a low price. These miniature satellites provide them a low-cost platform for many types of mission, including planetary space exploration, Earth observations, fundamental Earth and space science.

As it can be seen on the left graph in Figure 2, the number of these satellites launched every year has considerably increased since 2012 and the number of announced launch for this year has exploded. Nowadays, about a hundred of CubeSats are sent to space per year. So this is an important part of the space industry. And the graph on the right shows the repartition of the organization types, and indicates that universities are well a major actor. [4]

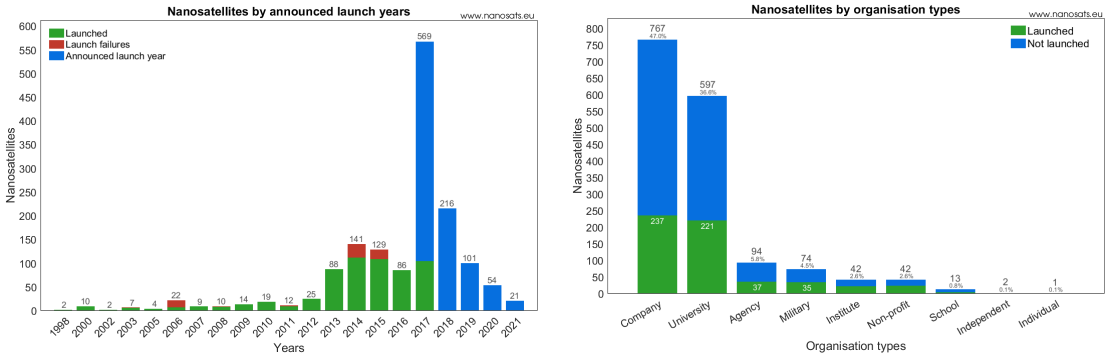

Figure 2: CubeSat information

2.2 Interferometry in space

The angular resolution of a telescope depends on the ratio between the wavelength observed and the diameter of the mirror. Therefore, it is necessary to increase the diameter of the telescope to improve the precision of the images obtained. However, the payload that can be launched with a satellite in space is limited, especially for CubeSats, so the size of the mirrors has a maximal value. It is the reason why some techniques have to be used in order to get images as accurate as possible with small telescopes.

One way to proceed is to use interferometry with several telescopes placed in orbit. Interferometry is a technique in which waves are superimposed causing the phenomenon of interference in order to extract information. An astronomical interferometer is an array of separate telescopes that work together, as a single telescope to improve the resolution by means of interferometry. Theoretically, it can produce images with the same angular resolution as a huge telescope with an aperture equal to the diameter formed by the separated telescopes.

In this project, the technique of optical aperture synthesis is used, which is a type of interferometry. It consists in mixing signals from different small telescopes to produce images having the same angular resolution as an instrument of the size of the entire collection. The whole system forms a Multiple Aperture Optical Telescope (MAOT).

So far, interferometry has been mostly used on ground, notably in big projects such as the Very Large Telescope (VLT) in Chili. For a number of years, astronomers responsible of the Earth observation have constantly increased the diameter of their instruments to improve the resolution. Unfortunately, increasing diameter of space telescopes comes up against technological and financial limitations. As a consequence, optical aperture synthesis appears like an attractive idea. It allows to compensate the distance of space telescopes in geostationary orbit by increasing the diameter and reaching resolutions unequalled for this orbit. Thus interferometry has a lot of interests for satellites and especially CubeSats because it would allow to have a very good resolution with small mass launched.

However, interferometry has not a long history in space. Indeed, these instruments require an optical path length accuracy in the order of a few nanometres across structural dimensions of several metres. This puts extreme demands on static and dynamic structural stability. Nevertheless, projects have already been developed, and a few scientific space missions based on interferometric instruments are currently under development in the United States as well as in Europe.

Darwin is a cancelled project of the ESA (European Space Agency), whose goal was to detect Earth-like planets orbiting nearby stars and search for evidence of life on these planets. Several spacecrafts forming a constellation were supposed to carry telescopes that would have redirected light toward a central satellite. Then, using a technique called *nulling interferometry*, the central star would be cancelled out and the planets would have become visible. But the program ended in 2007 because several more detailed studies were needed to assess the feasibility of such mission.

Another mission intended by the NASA was the Space Interferometry Mission, called SIM or SIM Lite, which was a supposed to be a space telescope hunting Earth-sized planets orbiting around other stars than the Sun. After being postponed several times, the project

was definitively stopped in 2010. The spacecraft would have collect and combine light with two mirrors and use interferometry to obtain precise measures.

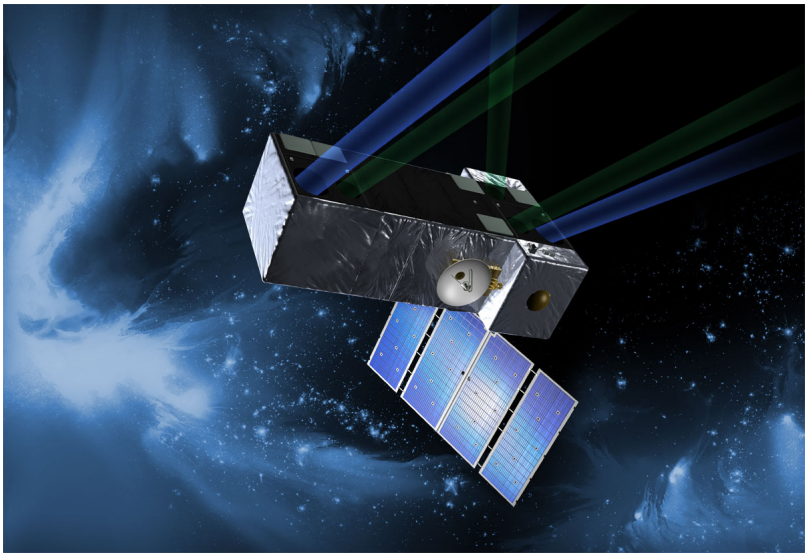

Figure 3: SIM Lite, artist view

Finally, interferometry in space seems to be really promising, but for different reasons very few missions have been realized and have not passed the project state. CubeSats are useful in this kind of situation because it allows to test at low cost the feasibility of a concept. In case of success of a space interferometry mission, it could be a scientific breakthrough because it would allow to take benefits from the low cost of CubeSats while having a good resolution of images.

2.3 Overview of the existing deployable structures

Since the beginning of space industry, plenty of deployable structures have been used. Indeed, the launchers capabilities limit the size of satellites, and build larger launchers is not a realistic option. This is especially the case of space observatories whose telescopes size is limited. Thus solutions have to be found to overcome this issue.

There are possibilities like the implementation of a formation flying mission or the assembling of a structure in orbit. However, the formation flying involve several problems, particularly for CubeSats. The fact that they are launched as secondary payloads limits the options for their deployment in appropriate constellation geometries. This problem is further aggravated given the current lack of propulsive options, which complicates the task of maintaining the spacecrafts in relative orbit formation. This is why the use of self deployable structures is a much more appealing solution, that is chosen for this project.

Due to their size specifications, small satellites in particular need deployable parts in order to achieve focal length long enough or for other purposes. Unfortunately, it is generally not possible to directly scale down existing deployable structures from larger spacecrafts. So for the small satellites, new deployable techniques have to be implemented. In particular, they have to present the characteristics of high packing ratio and low mass.

Here is a review of existing deployable structures with some field of applications, and of deployment mechanisms with comparison of their performances. Finally, the goal is to make a selection of the most appropriate solution for the aim of this study. The retained deployment method should present the abilities of reliability, rigidity and repeatability. Besides, it has to be compatible with CubeSats and thus have a sufficient packing ratio.

2.3.1 Typical deployable structures

The first kind of deployable structures is the solar panels. Having removable solar panels allows to increase the available on-power for a CubeSat which is basically limited. Indeed, the small dimensions of CubeSats restrict the area of solar panels, and consequently the power produced. Using deployable panels permits to stack several panels on top of each other until deployment in orbit, and by this way increase the area of solar array. Moreover, a manoeuvring capability can be added to the solar array so that they are able to follow the motion of the Sun, which improve the performances of the system.

Hinges with a self locking mechanism are generally used to ensure the good expansion of the panels. For convenience, the deployment is generally passive and actuated by springs.

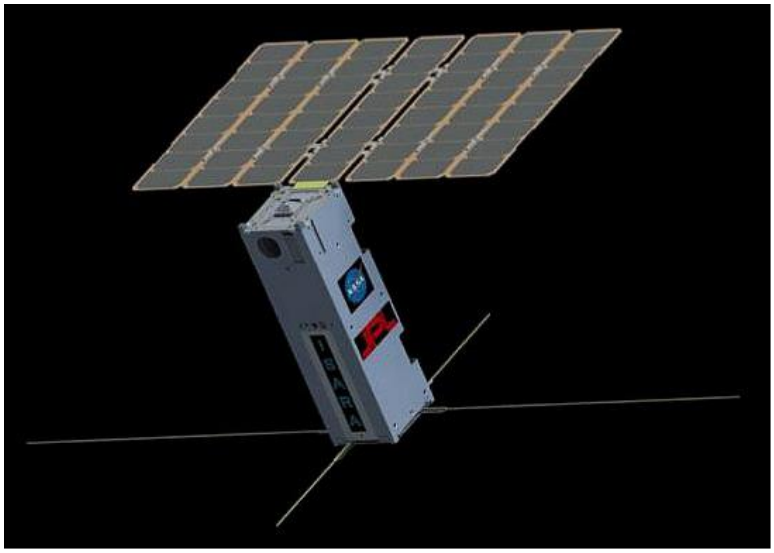

Figure 4: ISARA deployed solar panels

Figure 4 shows the 3U CubeSat ISARA, from NASA/JPL with its deployed solar panels. [5]

Then, other common expandable structures for satellites missions are the unfurlable reflectors antennas. There are mainly three different types of deployable antennas: [6]

- Mesh antennas,
- Solid surfaces antennas,
- Inflatable antennas.

The first one is the most common, with a reflective surface composed of knitted lightweight metallic mesh, which is discontinuous. It can reflect radio frequency waves up to about 40 GHz.

Secondly, solid surface antennas consist generally of a central hub with rigid curves panels arranged as radial petals. Antenna applications operating at frequencies over 40 GHz require high surface accuracy that offer solid surface antennas.

And the last category, inflatable antennas, give the smallest package ratio and mass. They are constructed from a thin flexible material which is folded before the launch and then deployed once in orbit by inflation. It is stiffened by an inflatable torus along the edge, but the main disadvantage is the difficulty of achieving high shape accuracy for the reflective surface.

Concerning CubeSats, antennas have generally to be adapted. Solid surface type involve generally a mass beyond the limitations of small satellites, while inflatable antennas are more adequate. Due to the enhancement of technology and launch opportunities for CubeSats, a wide variety of missions deeper into space are now enable. Hence, data communication rates become an issue, imposing the use of a parabolic deployable antenna adapted to small satellites.

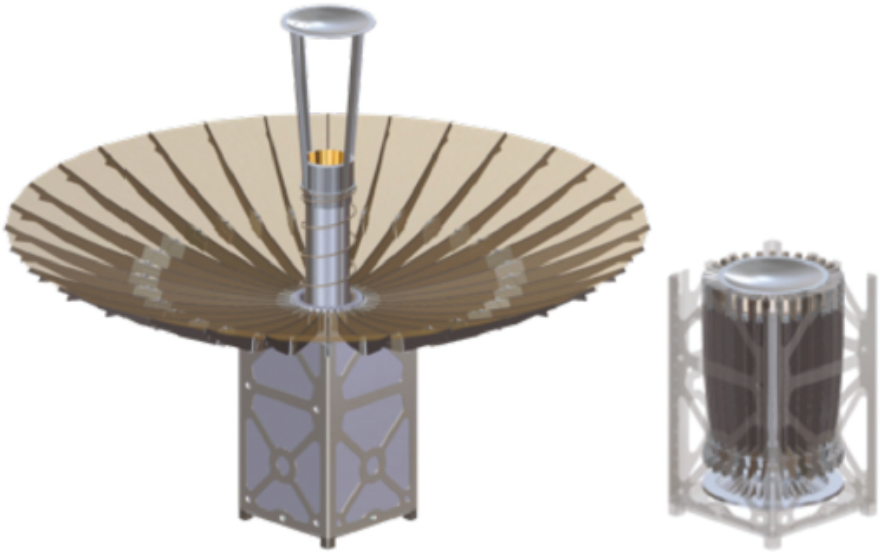

Figure 5: Ka-band parabolic deployable antenna

An example of this kind of parabolic deployable antenna is the KaPDA which has been developed by the NASA. This is a promising approach for providing a Ka-band high gain antenna that would increase by approximately a factor 100 the the data communication rates over an S-band high-gain antenna. It is visible in Figure 5, and has a folding rib architecture and dual reflector Cassegrain design. The antenna is designed with deeps ribs, precision hinges and a denser and stiffer mesh. The antenna and the deployment mechanism hold in a 1.5U. So KaPDA is an innovative antenna that creates opportunities for new CubeSats missions further into deep space, including potential interplanetary travel. [7]

Another type of deployable structures suitable for CubeSats are the solar sail deployer mechanisms. The first ever solar sail in orbit was the IKAROS, successfully launched by the

JAXA in 2010. Then NASA Marshall Space Flight Center developed the solar sail Nano-Sail-D, the first American solar sail in orbit which is illustrated in Figure 6. These satellites had different purposes, for Nano-Sail-D the main objective was to demonstrate the deorbiting capabilities of a large low mass high surface area sail. But the ultimate goal of the majority of solar sails, like for IKAROS, is to use solar sailing as the main propulsion. This technique uses the radiation pressure exerted by sunlight on a large surface to drive the satellite.

This would offer the possibility of low-cost operations, combined with long operating lifetimes. Moreover, it would allow to make any launch window virtually possible which is not the case with the only chemical propulsion. And this would be very useful for CubeSats which are deployed as secondary payload and thus must remain flexible. This technique does not use any propellant and is really interesting for the CubeSat industry.

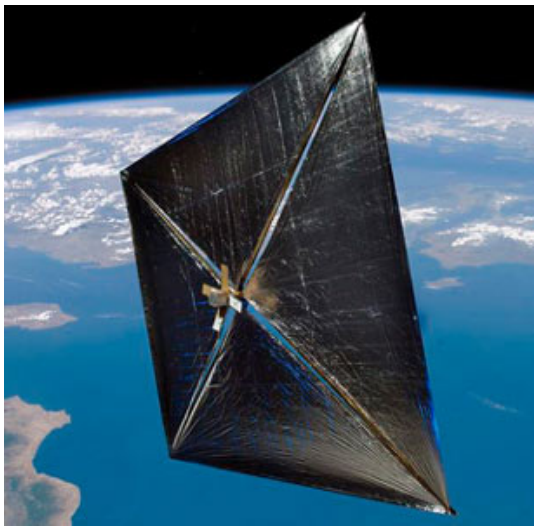

Figure 6: NanoSail-D in orbit

Furthermore, deployable sails can have many other applications different from solar propulsion such as the Nano-Sail-D. Currently, the space debris are a problem that concern the space industries. Indeed, their rising population increases the potential danger for all space vehicles and more specifically the ISS and other space stations. It is the reason why de-orbiting sails are now developed. They consist in a sail deployed from the spacecraft that increase the drag to more rapidly de-orbit the satellite, that disintegrates into the Earth's atmosphere.

Finally, a last widespread usage of expendable structure are the space telescopes. The small payload that can be placed inside a launcher limits the optical aperture size, and thus the resolution of the images. That is why deployable mechanisms are used to improve this resolution. This can be done in many ways.

First, it can be achieved with a longer focal length, if the secondary mirror is deployed to a certain distance from the main body. IXO (International X-ray Observatory) was a large satellite project developed as a joint effort between NASA, ESA and JAXA, which was cancelled in 2012. It was a X-ray telescope with an extension mechanism built to position the instrument from about eight meters as configured inside the launcher fairing, up to at least 20 meters to achieve the required operational focal length. The deployment sequence is shown in Figure 7, it is based on three articulated arms with motorized hinges. There is also

a locking system that keeps the mirror in its deployed configuration.

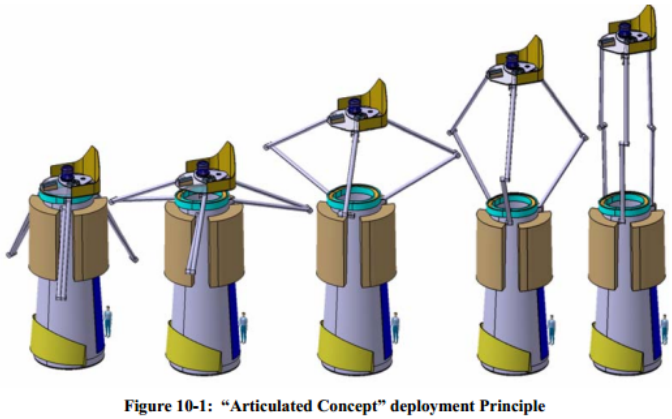

Figure 7: IXO deployment mechanism

Another possibility to improve the images resolution is to increase the area of the primary mirror which can be done using segmented mirrors. But this solution presents some difficulties, the first one is to achieve an very precise alignment for every mirrors in all degrees of freedom. The UK ATC has been developing a CubeSat sized deployable optical system with a primary mirror consisting in four square panels. In folded state, represented in Figure 8 it is contained in a 1.5U. Once deployed it gives a maximum baseline of approximately 300mm. So the petal mirror allows to overcome the limitation of aperture size due to the physical dimensions of the satellite. [8]

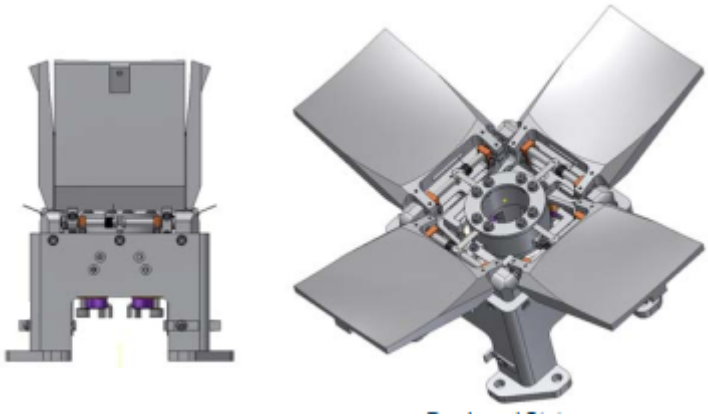

Figure 8: Segmented mirror in folded and deployed states

2.3.2 Different techniques of deployment

In the previous section, different types of deployable structure have been described without detailed information about the technique used for the deployment. Here is a non-exhaustive list of the main categories of deployable booms, masts or equivalent mechanisms that can be used to deploy a structure. Examples are also given, with the main characteristics of each category. After that, one of them will be chosen for this project.

For this study, the extendible part should be similar to a boom or a mast, regarded the required application. Booms have a lot of utilization in space missions, they are generally used to move away specific payloads at a certain distance of the satellite. For instance, a magnetometer can be departed from the main body in order to avoid interactions with the magnetic field environment of the spacecraft. Here the booms would be used to deploy the telescopes away from a central detector.

Articulated structures

Articulated structures have already been used with success on several missions. This category includes all the deployable structures using hinges, which can be passive or active. Basically, only a single active joint between two booms is necessary. Concerning the motorization either active hinges can provide the required actuation torque or the deployment can be passive, using the energy stored in torsion springs and passive hinges. An example of this type as already been given before with the IXO satellite.

But the articulated structures can take other forms, such as spring-loaded pantograph arms. This technique has already been used on FalconSAT-7, a nanosatellite designed by students of the USAFA whose goal is to deploy a membrane photon sieve from a 3U CubeSat to image the Sun. It produces high-quality image by diffraction through billions of microscopic surface indentations of the membrane. [9]

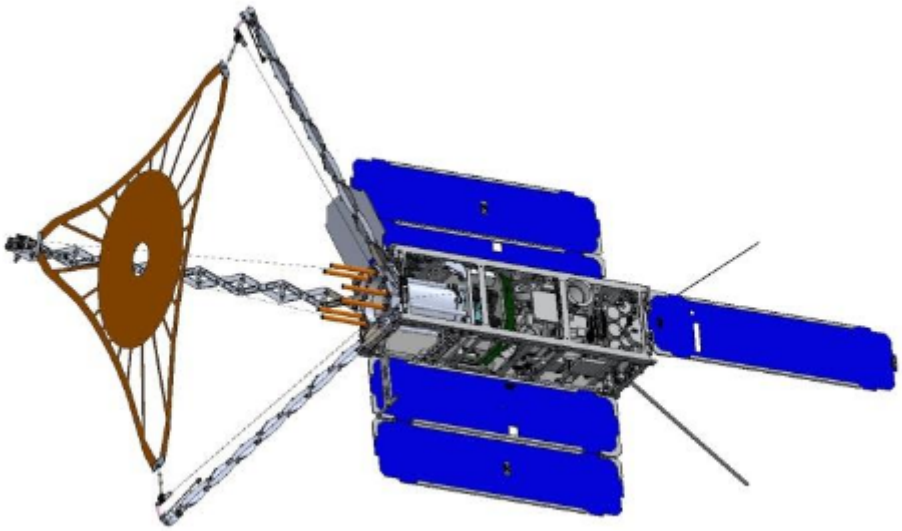

Figure 9: FalconSAT-7 with deployed pantograph arms

The deployment system is based on two stages spring loaded deployment mechanism. During launch, the membrane and the three paragraphs are kept inside a 1U volume closed by a door. When it opens, the support and deployment structures are moved to the top surface of the bus and then the three spring-loaded pantographs deploy the structure to the deployed configuration, which is shown in Figure 9. The pantograph arms put tension on the membrane photon sieve and ensure a high-quality imagery.

So this deployment technique is relatively simple and reliable, with a rigidity and a packing ratio that are satisfactory. But it requires a quite heavy structure, and thus has mainly been developed for large satellites.

Articulated truss and coilable masts

These are truss-like structures containing a number of pinned joints instead of rigid joints to provide several degrees of freedom for storage and deployment. They have a great extension, up to several tens of meters with a relatively compact storage volume and have a high reliability coupled with a long heritage deployment system. But they have mechanically complex designs and a huge mass, partially due to their deployment-control systems. This is the reason why they have mainly been used on large spacecrafts, at the ISS or even in the past on the American Space Shuttle.

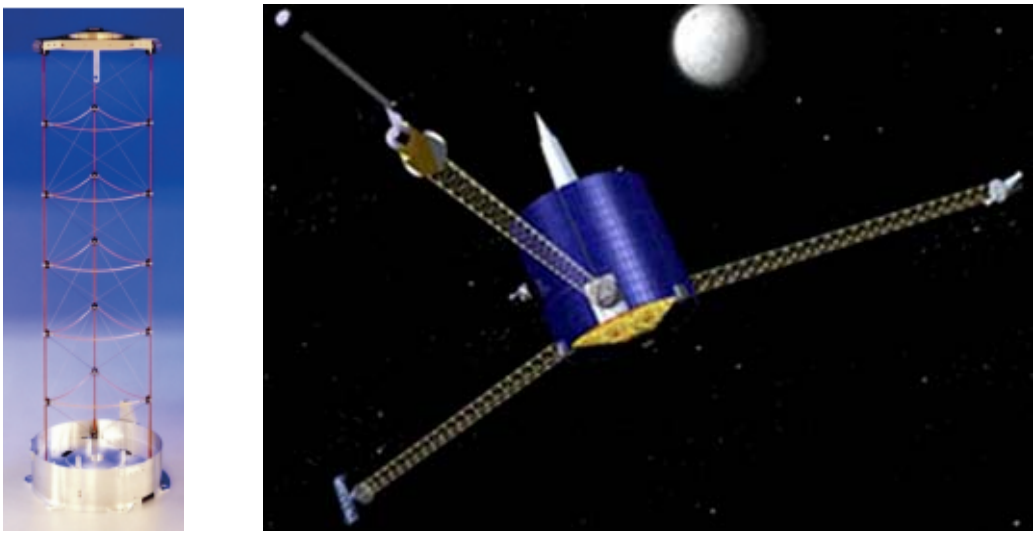

Figure 10: Orbital ATK Coilable boom & Lunar Prosector Mission

Orbital ATK is a company which is world leader in deployable structures technology for all Earth orbiting, planetary and deep space applications. They develop Coilable Boom Systems that have been successfully used on several missions like the Cassini or Lunar Prospector, represented in Figure 10. Typical applications include telescope optics deployment, such as high-precision focal length, to very large spacecraft payloads deployment of more than 100 meters. [10]

Concerning the applications on CubeSats, it has seldom been used. Yet, PRISM satellite from JAXA is one of the small satellites example. It deploys a 800 mm extensible boom supporting a lens. Before launch it is coiled and clamped to the main structure, then the fixations are unlocked and it deploys with its own elasticity. The sequence is shown in Figure 11. The structure is composed of longerons made in CFRP that stop the extension. [11]

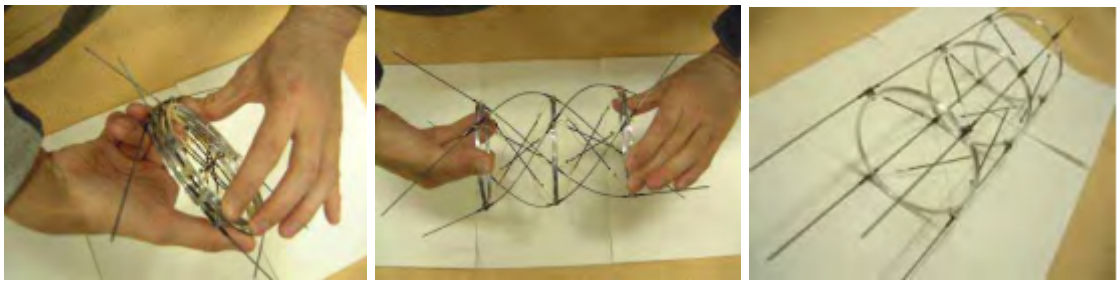

Figure 11: PRISM deployment sequence

Coilable Booms

These booms use morphing structures that exist in two geometrical states, one for the stowed and one for the deployed configuration. Made in carbonfiber, they can be spooled on a hub without damages or degrading effects in the form of a flat ribbon. The deployed boom can present different section, notable examples are : [12]

- STEM : Storable Tubular Extendable Member,
- CTM : Collapsible Tube Mast,
- TRAC : Triangular Rollable And Collapsible.

Figure 12: Examples of Coilable Booms

They have a long flight heritage but only for deployment of low masses. Their main advantage is their enormous compactness. Moreover they have a very long extension, up to 100m. But their deployment is less precise than other techniques, as well as their stability.

As a consequence, they are perfect for deployment of light structures such as solar sails, besides they have been used on the NanoSail-D. For this 3U CubeSat, four booms each one 4m long have been used to deploy the sail.

Inflated booms

This category features plenty of advantages : a very high packing ratio and extremely lightweight structure. Once rigidized, the structure has also a rather good rigidity. However, they can only deploy light loads and have a low deployment accuracy and post-deployment stability.

Concerning their functioning, the tubes have first to be inflated by a gas. After that, to maintain the structural rigidity for missions during later than a few weeks, the inflatable skin has to be rigidized. Several techniques exist for this process such as U-V setting resins, thermosetting resins solvent boil-off rigidization or foam rigidization. [13]

An inflatable rigidisable cylindrical mast of 1 meter was developed for the InflateSail project. For that mission, the boom was rigidised by removing the residual creases in the aluminium-laminate skin material through strain-rigidisation, to ensure long-term structural performances. This satellite is a 3U CubeSat launched for a demonstration missions of a drag deorbiting sail of 10 m^2, which is visible in Figure 13. [14]

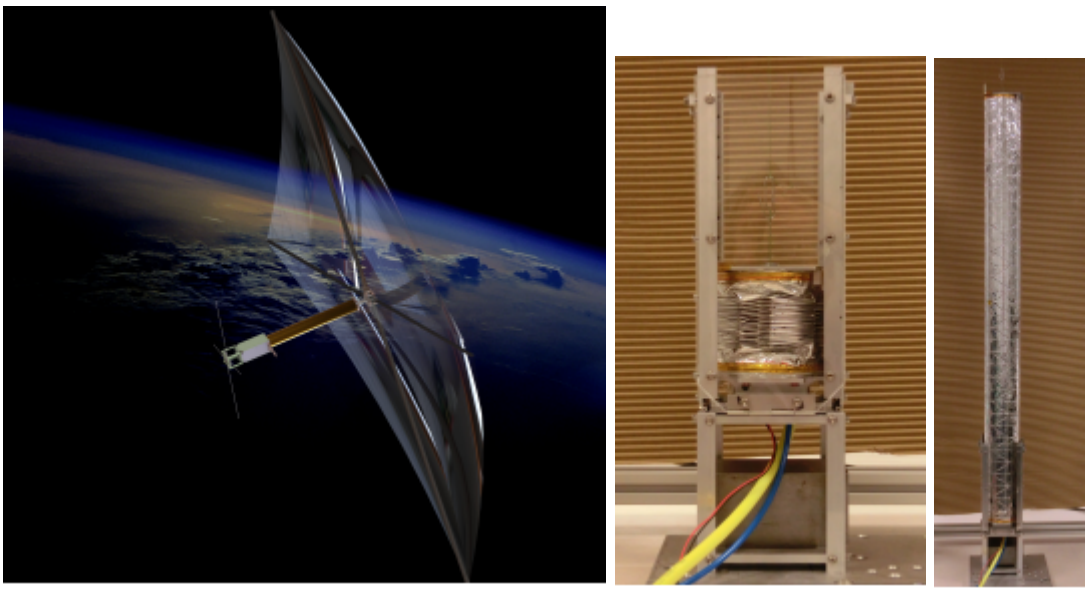

Figure 13: InflateSail satellite & boom in stowed and deployed configuration

On this figure, the inflatable cylindrical mast is also represented in its stowed and fully deployed configuration. Deployments test have been achieved and showed a repeatable deployment with minimal deviation from the intended straight path.

In summary, inflated booms are recommended for the deployment of light structures, typically membranes under 10kg such as solar sail. Their very high compactness make them attractive for CubeSats. But due to their lower deployment precision they have less been used for telescopes and mirrors structures.

Tape-spring based structures

This kind of boom uses EMC (Elastic Memory Composite) as an alternative to classical joints. An EMC is first folded by applying heat and force above its glass transition temperature, then cooled below the transition temperature retaining the folded shape. The material returns to its original unfolded shape if reheated above the transition temperature. They have the ability of high-strain packaging and shape-memory effect, and have therefore widely been used for satellite applications.

Typically, EMC are used instead of hinges. Tape-springs or Carpenter tapes can be

used to connect several tubular segments. So they are self-deployable, using the movement is guided by the tape springs that return in their initial configuration. Both folded and deployed configurations of tape-springs can be seen the right picture of Figure 14. They are also lightweight and have a rather good packing efficiency. But here again the post-deployment stability as well as the accuracy are not guaranteed. Self-deployment mechanisms are appreciated because they permit to reduce the complexity and the cost, and they decrease the space taken by the structure.

Figure 14: Stowed configuration of a tape-spring boom

The stowed configuration of such a boom is represented in Figure 14, three tubular segments are linked by folded tapes for total a deployed length of 4 m. This structure has been used on FalconSAT-3, a small satellite developed by the USAFA, with the aim of extend the moment arm of the Micro-Propulsion Attitude Control System. [15]

Actually, their application has only been envisaged for nanosatellites, to deploy light structures. Indeed, they cannot deploy heavy payloads and have not been really developed on large satellites.

Telescopic booms

Finally, telescopic booms consist of concentric tubes that are deployed sequentially, one after the other or symmetrically, all the tubes in the same time. They are generally made of CFRP or aluminium. This solution is much stiffer than other deployable techniques, besides being more precise and stable. Nevertheless, the deployment mechanisms are much heavier and have a low packaging ratio. Telescopic tubes are generally used to move a payload away from the spacecraft.

They have been widely used for large satellites, and different companies manufacture and sell their own product, such as the Astrotube Max from Oxford Space Systems or the Telescoping Boom of Orbital ATK. [16]

The extension can go up to several dozen meters and they are generally retractable. They have a long heritage of deployment system, with different types of motorization already

tested. However, they have been very little used on small satellites.

Nevertheless, at least one telescopic tube has already been used for a CubeSat mission : QuakeSat. This nanosatellite was developed in collaborations of Stanford University and the QuakeFinder Team of Palo Alto, in California. Its primary mission was to detect and record ELF (Extremely Low Frequency) magnetic signal data in order to develop a technique to predict earthquake activity. A telescoping boom was extended and carried a magnetometer 30 cm away from the satellite, as it can be observed on Figure 15. [17]

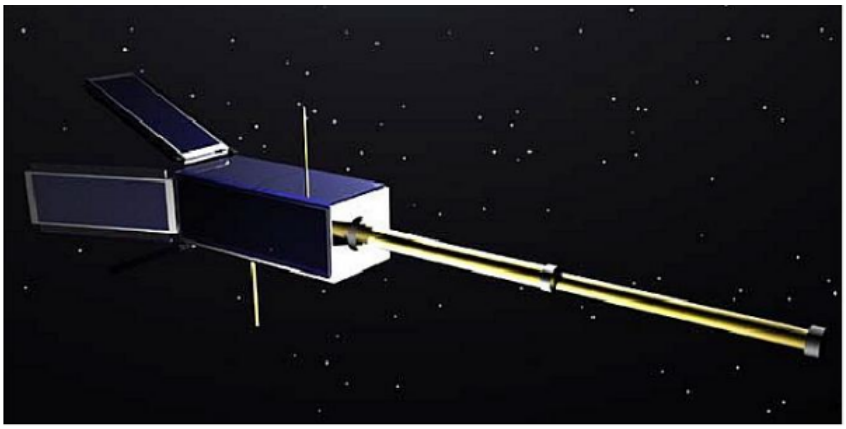

Figure 15: QuakeSat deployed telescopic boom

2.3.3 Summary of the possibilities

All the possibilities of deployment techniques presented have specific characteristics and cannot be used in all circumstances. This study has the objective to deploy telescopes and therefore requires the most precise and reliable extension coupled with a very rigid deployed structure. Moreover, the selected choice must be compatible with the CubeSat norms of mass and size, so must present an acceptable packing ratio.

To summarize the different options, Table 2 give examples of missions and their main characteristics. When the precision of deployment is available, it is written, as well as the deployed length. As explained before, tape-spring based and inflated structures can deploy only very light payloads and for this reason no large satellites missions are mentioned in the table.

Deployment methods	CubeSats & microsatellites		Larger satellites	
Articulated Structures	Falcon Sat-7:	• spring-loaded pantograph arms • unknown precision	NuStar [18]:	• Articulated Mast System • Orbital ATK product • 60m length deployed • accuracy < +- 1.3 mm
Articulated Truss (and coilable masts)	PRISM:	• 19.2 x 19.2 x 40 cm (+- 16U) • 0.8m deployed length • unknown precision	K-truss boom[19]:	• Sierra Nevado Corporation product • 101.5 inch length deployed • unknown precision
Coilable Booms	AlSat-Nano[20]:	• Astro Tube • Oxford Space System product • 2m length deployed • 0.5U stowed volume • accuracy of +- 0.1mm	GeoLITE[21]:	• Northrop Grumman product • unknown precision
Inflated Structures	InflateSail[14]	• CubeSat 3U • 1m length deployed • unknown precision	/	
Tape-Spring based	FedSat[22]:	• cube of +- 60 cm size • 2.5m length deployed • unknown precision	/	
Telescopic Tubes	QuakeSat:	• deployed length of 3 x 350 mm • unknown precision	Space Telescopic Boom [23]:	• collaboration from COMAT & CNES • 2.7m of deployed length • precision of 1.5 mm

Table 2: Summary of main deployable missions characteristics

2.4 Preliminary design of the satellite

In order to select one of the techniques presented, it is necessary to realize a preliminary design of the spacecraft and to evaluate the space devoted to the deployment system.

In this study, several telescopes are placed inside a same CubeSat, but the strict dimensions imposed limit the number of telescopes that can be used. So only two are used to collect the light and to return it towards a central part, where it is directed and recombined on a detector placed. Thus the spacecraft should be divided in three parts once in orbit, and two different deployment system have to be implemented.

However, in case of success it is possible to consider in the future a mission with more than two telescopes, with a similar deployment system.

Actually, two different optical designs can be envisaged for a MAOT.

- the *Fizeau* design (fig. 16a): the aperture segments are portions of a unique primary mirror. The length L is close to the maximum baseline B.
- the *Michelson* design (fig. 16b): independent telescopes are combined by a dedicated telescope. The length L is close to the telescope diameter D.

Here, the configuration selected is from the family Michelson, with two independent telescopes that are deployed to increase the length B of the maximum baseline.

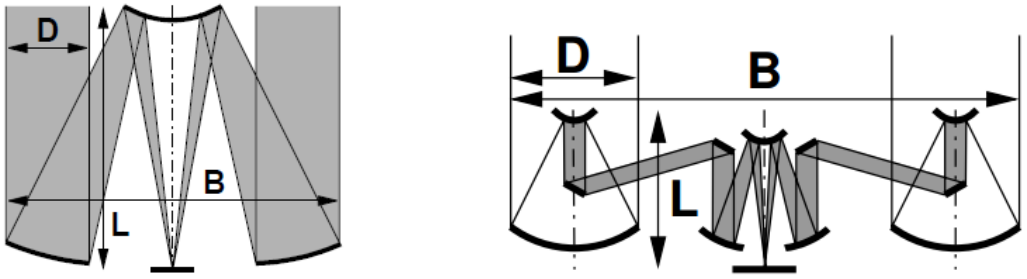

(a) Fizeau configuration (b) Michelson configuration

Figure 16: Different configurations of Multiple Aperture Optical Telescope

2.4.1 Design of the telescopes

To achieve a configuration with two collecting telescopes and a central recombination system with the detector, a CubeSat 6U is needed. Indeed, the telescopes used to collect the data must ideally fit inside a 1.5U, 15cm x 10 cm x 10 cm. They are based on the master thesis of Christian Kintziger, a feasibility study of a UV imager about a CubeSat platform. [24]

Actually, 6U satellites present many interests : the dimensions allow to have larger aperture for telescopes while still maintaining compatibility with existing CubeSat accommodations standard.

So the idea is to place the two external telescopes and the central part inside three different CubeSat 2U, forming the 6U. These CubeSats are maintained together during launch, and then deployed once in orbit. Actually, this concept of several part tethered in one unique

CubeSat has already been experimented. Indeed, the MAST (Multi-Application Survivable Tether) was a CubeSat mission that was launched to demonstrate space tether survivability.

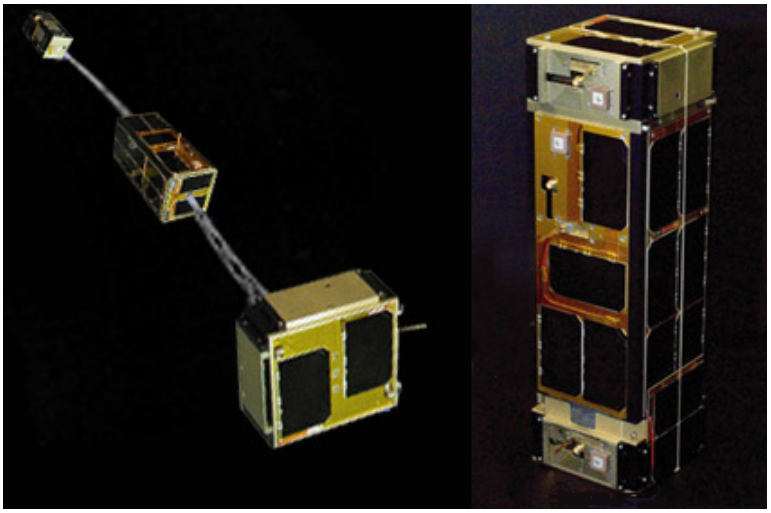

Figure 17: MAST in launch and deployed configuration

The MAST satellite consisted of three CubeSats 1U stack together for launch inside a P-POD deployer, that had to deploy once in orbit. The same concept can be applied for this work, with three CubeSats 2U stacked to form a unique CubeSat 6U.

In the work of Kintziger, the optic design was a Cassegrain-type with 15cm between the secondary mirror and the detector, which is in the context of this study replaced by a mirror inclined at 45°, used to sent the incoming signals to the central detector. The primary mirror has a diameter of 95 mm and the secondary of 20 mm. The Figure 18 shows the 2D and 3D views of these mirrors.

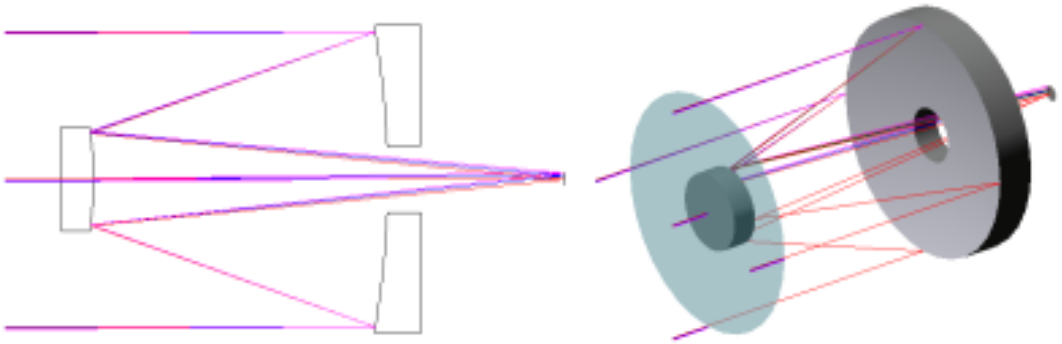

Figure 18: Mirrors design

Actually, this telescope shall be adapted to become afocal as required by the Michelson design, but it is assumed here that the overall envelope and shape remain similar. To produce an afocal telescope, it is necessary that the primary and the secondary mirrors have the same focal point so that incoming light is sent toward the center in straight parallel rays.

Concerning the central system, it can be exactly similar to the one represented in Figure 18. Here, the signals have to be focused on one point, where the detector is located. The entire system, with a representation of the path travelled by light is shown in Figure 19.

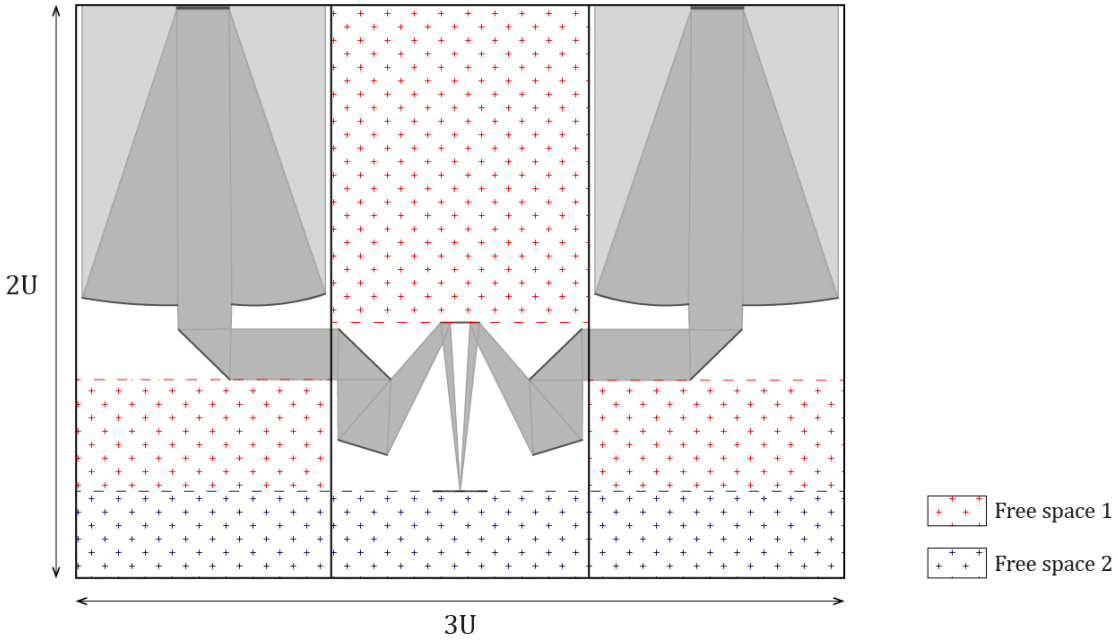

Figure 19: Mirrors configuration

This primary design of the agencement of the CubeSat provide an idea of the free space left by the optic system. This space is divided into two parts that are dedicated to different functions. One part of this space is occupied by all the components necessary for the sustainability of the spacecraft, which are detailed in a further section, this is the part referenced by the legend as *free space 1* on the graph.

Finally, the *free space 2*, located in the bottom is devoted to the deployable system. This represents a box of 323.4 mm x 95 mm x 36.3 mm where the two deployable structures and their motorization should take place.

2.5 Choice of the deployment mechanism

Now that the different aspects linked to the deployment mechanisms have been considered, it is time to choose the one that will be used for this mission.

First, some solutions can directly be eliminated because they do not provide a deployment with enough precision, and thus are not suitable for this study. Indeed, as explained in the section 2.3.2, inflated booms and tape-spring based structures have the lowest deployment accuracy and thus cannot be retained.

Then, concerning coilable booms, they are used mainly to deploy very light structures such as solar sails and hence have to be rejected. They cannot deploy heavy masses and the deployed structure would have a low rigidity. So there are three possibilities remaining, which

present similar abilities, namely a high accurate positioning, a good rigidity and a sufficient packing ratio.

However, from the point of view of this last characteristic, all deployment techniques presented before are adapted for CubeSat dimensions. Besides, as seen in the preliminary design, there is enough space in the satellite for any kind of deployable structure, so that this argument is not decisive. Then concerning the accuracy of the deployment, there is too few data to be able to spotlight one of the three methods, which offer similar results. So that the decisive argument has to be the rigidity of the deployed structure.

This is the reason why, considering all of these arguments, the telescoping boom seems to be the best option and is retained for this work. Indeed, it combines good deployment accuracy with the most rigid deployed structure. The free place below the CubeSats is sufficient to contain the mechanism. There are different kind of motorization and locking systems that exist and have been successfully applied to different satellites. And finally, the mechanism is not too complex.

Moreover, it is an innovative solution, which has barely been used for CubeSats. But several companies study telescopic tubes for larger satellites, and thus this technique seems promising.

3 Design of the satellite

Up to now, the deployable structure has been selected and a preliminary design of the spacecraft has been done. This first design determined the configuration and the positioning of the different telescopes and mirrors, and served to identify approximately the location of the different subsystems.

In the following, these systems are described and then the telescopic booms used for the deployment are detailed, with information about the design, the motorization and the locking mechanism.

3.1 Systems

As explained, a part of the free space left by the optics systems must be occupied by the different systems that are required for the good functioning of the satellite : the communication system, the attitude determination and control system (ADCS), the electrical power system (EPS) and the on-board computer.

These systems can be located everywhere in the spacecraft, far enough away from the others. So there shall be an electrical connection between the different CubeSats once deployed, so that all the elements can operating normally even if the power is on one side and the ADCS on another side of the satellite.

3.1.1 On board computer

The ISIS on board computer (iOBC) is a high performance processing unit based around an ARM9 processor with a speed of 400 MHz, making it one of the most capable on-board computer currently available on the market. It is a product essentially made for CubeSats, and is available in the CubeSatShop. Its dimensions are 96 mm x 90 mm x 12.4 mm, so it can be located in the free space below the telescope in one of the lateral 2U. [25]

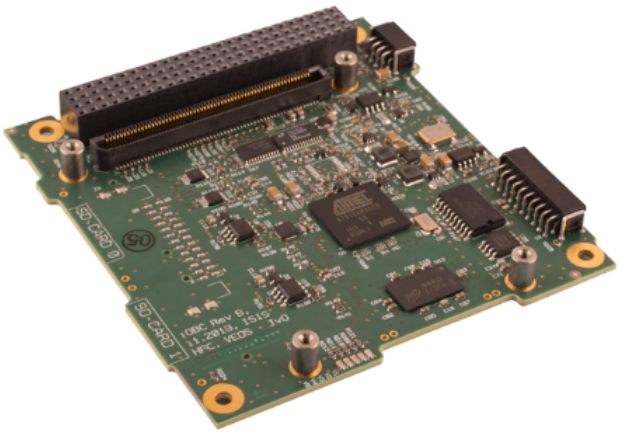

Figure 20: On board computer

The operating temperature of this component is comprised between -25°C and 65 °C, and the total mass of the iOBC is 94 g.

3.1.2 Communications

The ISIS TXS S-band transmitter is a CubeSat standard compatible transmitter module designed specifically for nanosatellite located in LEO, which is the nominal orbit of this satellite. It weights 62 grams with a form factor of 90 mm x 96 mm x 15 mm, so it will be located with the on board computer in the free space below one of the collecting telescopes. [26]

Figure 21: Communications system

3.1.3 ADCS

The iADCS400 is a fully autonomous attitude determination and control system aimed at small satellites with a 6U CubeSat form factor or similar. It is a joint development of Hyperion Technologies B.V. and Berlin Space Technologies GmbH. [27]

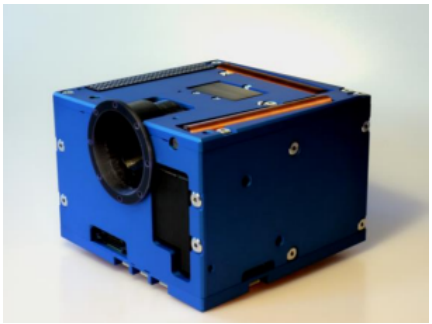

Figure 22: ADCS

It uses a star tracker for the attitude determination and reaction wheel RW400 with MTQ400 magnetorquers for the control of the satellite. Both spacecraft attitude controllers can be seen in Figure 23. It features also an optional precision MEMS gyroscope and can deliver a maximum torque of 2.5 mNm.

The mass is comprised between 1150 g and 1700 g, depending on the reaction wheel used. And the outer dimensions are 95.4 mm x 95.9 mm x 67.3 mm. So the only place where it

can be situated is in the central CubeSat 2U, above the telescope and the detector.

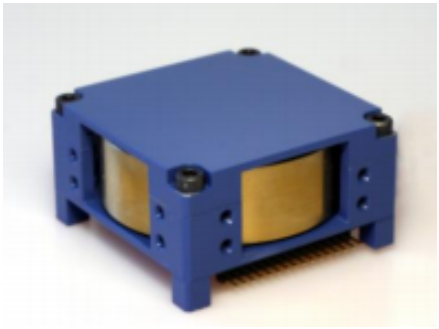

(a) Reaction Wheel

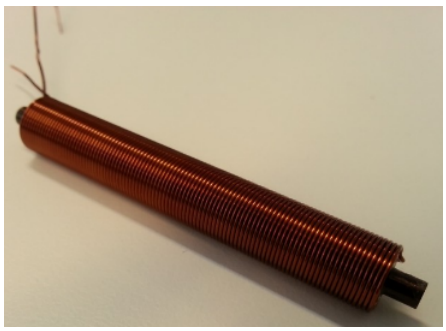

(b) Magnetorquer

Figure 23: Actuators included inside iADCS400

3.1.4 Electrical Power System

Finally, it is necessary to have a system to regulate the power of the spacecraft. The NanoPower P60 represented in Figure 24 is a modular power system suitable for large nanosatellites, and thus for CubeSats 6U. The dimensions are 92 mm x 88.9 mm x 30.4 mm and the mass is 370 g. It is located in the free space of the other lateral 2U, at the opposite of the other systems. So the deployed CubeSat should have an electrical connection linking each of the three parts. [28]

Figure 24: Battery

Observations are only made when the Sun is visible, when power generation is not a problem. So batteries are not needed for this CubeSat. This EPS system contains a P60 Dock motherboard and a combination of an Array Conditioning Unit (ACU) and Power Distribution Unit (PDU) daughterboards.

3.1.5 Solar Panels

ISIS offers a range of high performance CubeSat compatible solar panels, body mounted or deployable arrays which are supported for 1U to 12U sizes. It fits on all the CubeSat structures and subsystems, so there is no compatibility problems. They can be customized

to meet the needs and requirements of the mission. The solar cells are GaAs triple-junction and for a 6U CubeSat they can provide up to 17 W. [29]

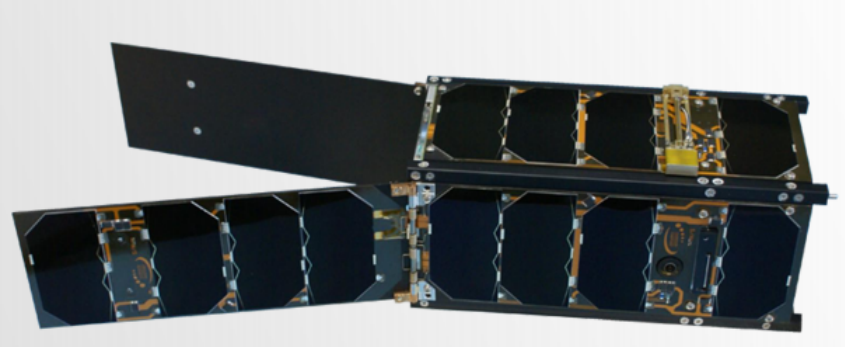

Figure 25: Solar Panel

Figure 25 shows deployable solar panels on a CubeSat 2U. In the stowed configuration, the panels are positioned outside against the structure. There is extra space there, provided for the panels. For this work, the panels can be disposed on all the sides of the CubeSat 6U, except the top and the bottom faces. So it means 8 panels of about 10 cm x 20 cm.

3.1.6 Thermal control

Thermal control can be done with passive or active methods, but for CubeSats passive method are preferred because of the lack of place. These methods can consist just in a coating applied on the surfaces or MLI blankets.

3.2 Deployable structure

The design of the two lateral CubeSats 2U that are deployed is shown in Figure 26, and takes into account the mirrors and the different systems introduced before apart from the thermal control and the solar panels. This model is made with the CAD software *Catia*. The central CubeSat is also represented in Figure 27.

As it can be seen, all these subsystems can be located in the *free space 1* of Figure 19. Moreover, it remains some place between the EPS system and the inclined mirror that can be useful for further application. And the deployable structure has as expected a free space of 323.4 mm x 95 mm x 36.3 mm where it takes place. Thus the solution retained, the telescopic tubes, can have a maximal diameter about 30mm.

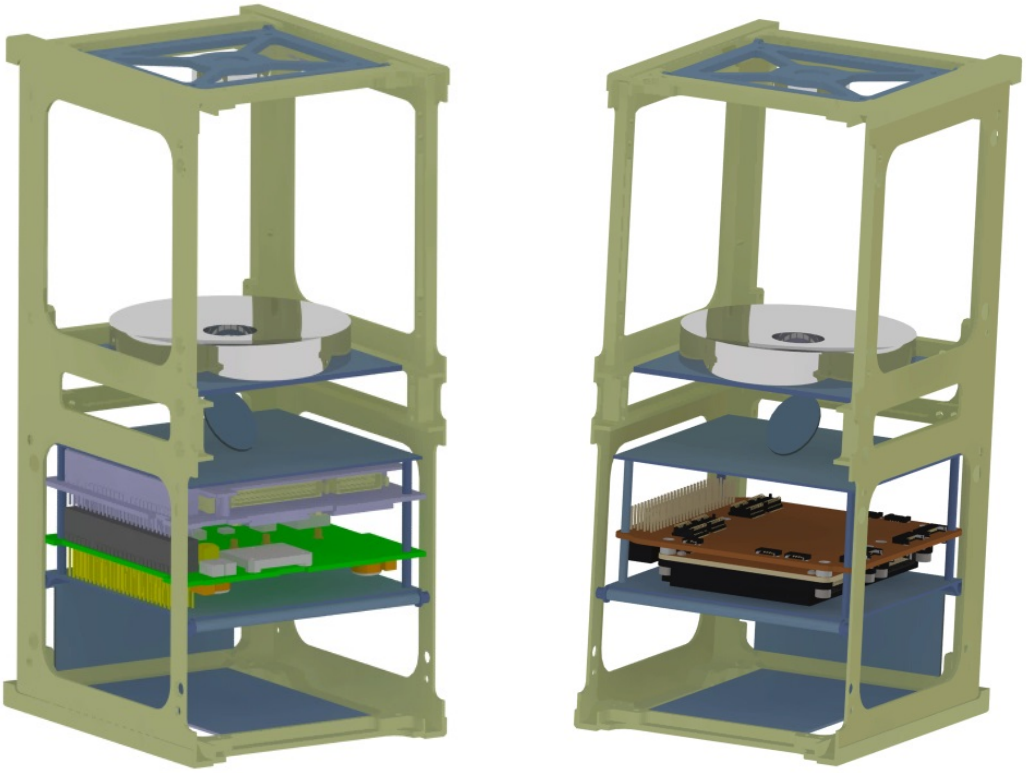

Figure 26: CAD model of the external CubeSats 2U

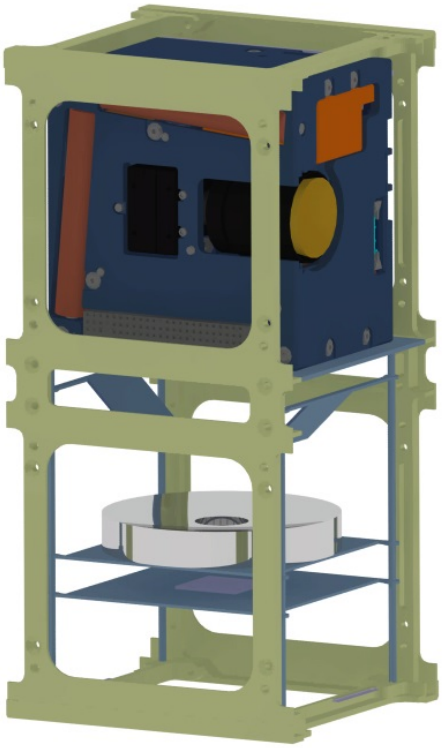

Figure 27: CAD model of the central CubeSat 2U

Then starting from the external diameter, it is possible to determine the diameter of the inner tubes. If a thickness of 1mm is considered for the structure with a gap of 2mm between two consecutive tubes, where the locking and the sliding mechanisms take place, it gives the successive external diameters :

	Diameter [mm]	Length [mm]
Tube 1	30	203.2
Tube 2	24	201.2
Tube 3	18	199.2

Table 3: Sizing of the telescopic tubes

To maximize the deployed length, the tubes are situated in the initial configuration inside two consecutive CubeSats. They are constructed in aluminium, as it was done for the QuakeSat mission, using concentric tubular sections.

Concerning the number of tubes, there are two possibilities that might be considered : a boom with two tubes or three tubes. The first option gives a greater rigidity to the deployed structure but the second choice increases the deployed length and so improves the resolution. In order to make a decision with as much information as possible, the two different configurations will be compared in the following sections to determine exactly what they involve.

An ever longer boom could be possible with a fourth tube. But then the diameter of the element added would be only 12mm, which is relatively small, and the deployed structure would be more flexible. So this option is not considered.

From the point of view of the deployed length reached, two tubes give a total of 675 mm while three tubes reach about 1050 mm. This distance corresponds to the length between the two lateral extremities of the CubeSat, the distance B of Figure 16b. The dimensions of each tube are given in Table 3. The length of the first tube corresponds to the distance between the sides of two consecutive CubeSats 2U in the stowed configuration. And the length of the other tubes is slightly smaller, so that they are not in contact in their initial position.

Hence, there are two parallel deployment systems, one for each telescope. And the two telescopic booms are positioned side by side in the central CubeSat.

3.2.1 Tribology

Before getting to the heart of the main topic that is the mechanism of the telescopic boom, it is essential to remind the importance of tribology for space mechanisms.

Indeed, phenomena of friction and wear, as well as the need of lubrication are fundamental aspects of space mechanisms. These mechanisms need to be more sophisticated and reliable, to have a longer life than conventional ones. In fact, they are confronted to the space which is a hostile environment where the lack of oxygen encourages metallic surfaces to weld together, where extreme temperatures are experienced. In addition they are subjected to severe vibrations during launch.

On ground, clean metallic surfaces react with the atmosphere to form oxides, nitrites and other chemical components which adhere to the surfaces by weak and strong chemical forces.

These layers act as protective films such as two metallic surfaces are not directly in contact but protected by a third body. However, under vacuum, these films which could exist in the beginning tend to disappear by evaporation or friction and are not regenerated after their removal. So two metallic surfaces which have been cleaned adhere to each other by molecular diffusion. This phenomenon is called *cold welding*.

Cold welding risks are increased in different conditions, for instance in presence of two surfaces with the same crystal structures or which have natural films that are easily removed. So surfaces must be protected by films which improve friction conditions and reduce risks of cold welding. It is the reason why tribology has a great influence in space structures.

Tribology is the science and engineering of interacting surfaces in relative motion. It includes the study and application of the principles of friction, lubrication and wear between moving surfaces. This science has a considerable importance for the reliability of satellites and is essential for anyone pursuing the design of space mechanisms.

The role of lubrication is to ensure the separation of moving parts with the aim of reducing the coefficient of friction, eliminate the risk of micro-welds and to minimize wear. In general, a lubricant is a solid, liquid or paste which is introduced in the gap between the parts in relative motion, and which has the objective to facilitate the motion. In this way, surfaces are protected against damage, war and tear. A careful consideration should be given to lubricants, because the space environment can lead to outgassing. And the loss of some of the lubricant by outgassing may result in insufficient quantity of product to maintain proper lubrication or to a deterioration of lubricants by the pollution of surrounding cold equipment.

Lubricants can be liquid (also mentioned as wet films) or solid materials (dry films), with greases placed in an intermediate category subjected to the same concerns as liquid lubricants. Each solution has its advantages and drawbacks and cannot be used in every cases. Wet lubrication will tend to evaporate and creep, which induce a loss of lubricant over time, by contrast they deliver less mechanical noise. While dry lubricants have poor thermal characteristics and can lead to debris which are likely to produce noise. However, they have fewer problems of creep and evaporation. [30]

Here are a few of the most used lubricants :

- wet lubrication :
  - ➢ Synthetic hydrocarbons : essentially Multiplied Alkylated Cyclopentanes (MACs)
  - ➢ Perfluoropolyethers (PFPE) : used nowadays but incompatibility with many metals
- dry lubrication :
  - ➢ Solid lubricant composites : based on polymers loaded with molybdenum disulfide (MoS_2) or PTFE (Teflon)
  - ➢ Soft metals: lead and gold are the most effective.

Actually, conventional lubricants used on ground are generally no longer suitable, since they evaporate or migrate easily (due to microgravity and creeping). For example, graphite is very used on Earth but is not suitable for space because it becomes defective at low pressure. In our case, the deployment of a boom, dry lubricants are more appropriate. So a choice has to be made between MoS_2 and PTFE, since soft metals have higher friction coefficients and

are thus rejected. [31]

Molybdenum disulfide, an agent extracted from mined ore, is an effective lubricant in high vacuum conditions. It has been the most used since the beginning of conquest of space, has a low friction coefficient and high loads limits of temperature service.

Teflon was created by DuPont Chemical Company and is now manufactured by various companies for many purposes. This material presents one of the smallest coefficients of static and dynamic friction.

In the following, the lubricants used and the tribology are investigated for all mechanisms, in order to ensure a good operation. For example, outgassing of materials is a major issue : the loss of some of the lubricant by outgassing may result in insufficient quantity of product to maintain proper lubrication, a deterioration lubricants by the pollution of surrounding cold equipment or by creep or dispersion with surface tension.

3.2.2 Motorization

Concerning the motorization of the deployment there are several solutions existing that can be considered.

Telescopic masts can be deployed with two different arrangements. The first way is sequentially so one tube after the other, what can be done with the spindle-and-nut technique represented in Figure 28(a). Or the tubes can be deployed synchronously using cables and pulleys, as shown in figure 28(b).

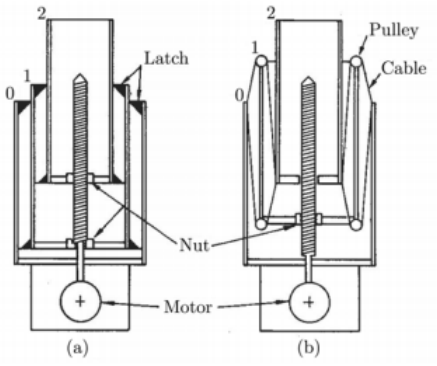

Figure 28: Telescopic motorisation

In our case, it is not necessary to have a synchronous deployment. Because this technique is more complicated to implement and hinges can introduce inaccuracies in the deployment. So a sequentially technique is used here.

Then, the deployment and the retraction can be controlled by various mechanisms. A central worm screw can be used to deploy the different tubes. Another technique consists in using a STEM actuator. This technique has been proposed by the NASA in 1994 [32]. Annular supports can be used to guide the STEM along the tube and to stiffen also the structure. A last technique suggested to deploy a telescoping boom was used by the satellite QuakeSat. Springs were compressed until release of the deployed structure, where they pushed the segments out. Each segment had its own spring, placed in the gap between two consecutive tubes.

These three solutions could probably work but a choice has to be made. Deployers from the STEM family are simple and lightweight, and they have been successfully deployed in space without failures. Besides, some companies like *Northrop Grumman* uses STEM as linear actuator since years. Therefore, a similar device is selected for this mission.

This actuator has a long flight history, which has begun in 1988 with the Hubble Space Telescope. They have several kind of deployer, and are currently working on a new prototype adapted for CubeSat : the NANO STEM, visible in Figure 29 [33]. This device is useful as CubeSat deployable or boom to drive a telescopic mast, so it could be used for the deployment of the telescopic tubes used in this project. This is a 0.163 kg deployer with a maximal push force of about 222.5 N, at limit load.

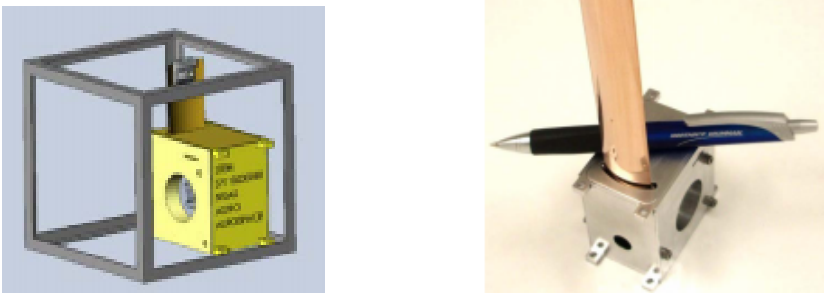

Figure 29: NANO STEM prototype

As it can be observed, this device stands without problem inside a CubeSat 1U volume. So it could be placed behind the telescopic tubes that have to be motorized, in the lateral CubeSats 2U. Concerning the expected deployment precision, it should be about 0.1 mm, which is the value obtained for the AlSat-Nano satellite which is a similar project.

3.2.3 Locking mechanism

In order to have a deployment as precise as possible the tubes have to be guided and a locking mechanism has to be introduced to keep the structure in the final position once deployed.

The CubeSat QuakeSat that deployed also a telescopic boom used a mechanism that is shown in Figure 30. Each segment of the boom has a capture ring which prevents the inner segment to separate from the previous. The inner tube has a slide bushing made in Teflon, which is the only part in contact with the outer tube. At the end of the course, it encounters the slide of the outer segment, and it locks as represented in Figure 31. As seen before, using Teflon allows to not use lubricant, and involve a mechanism complying with the space norms.

This mechanism is relatively simple, presents the advantage to act as slider and as a lock joint and its effectiveness has already been demonstrated by the success of the QuakeSat mission. Moreover, the sliders are made in Teflon which is usually used by the space mechanisms, as explained before. However, this kind of locking does not prevent the torsion of the tubes. And this could be disastrous because if the spacecrafts carrying telescopes rotate, it would

alter the observations. So another system should be introduced to counter this phenomenon.

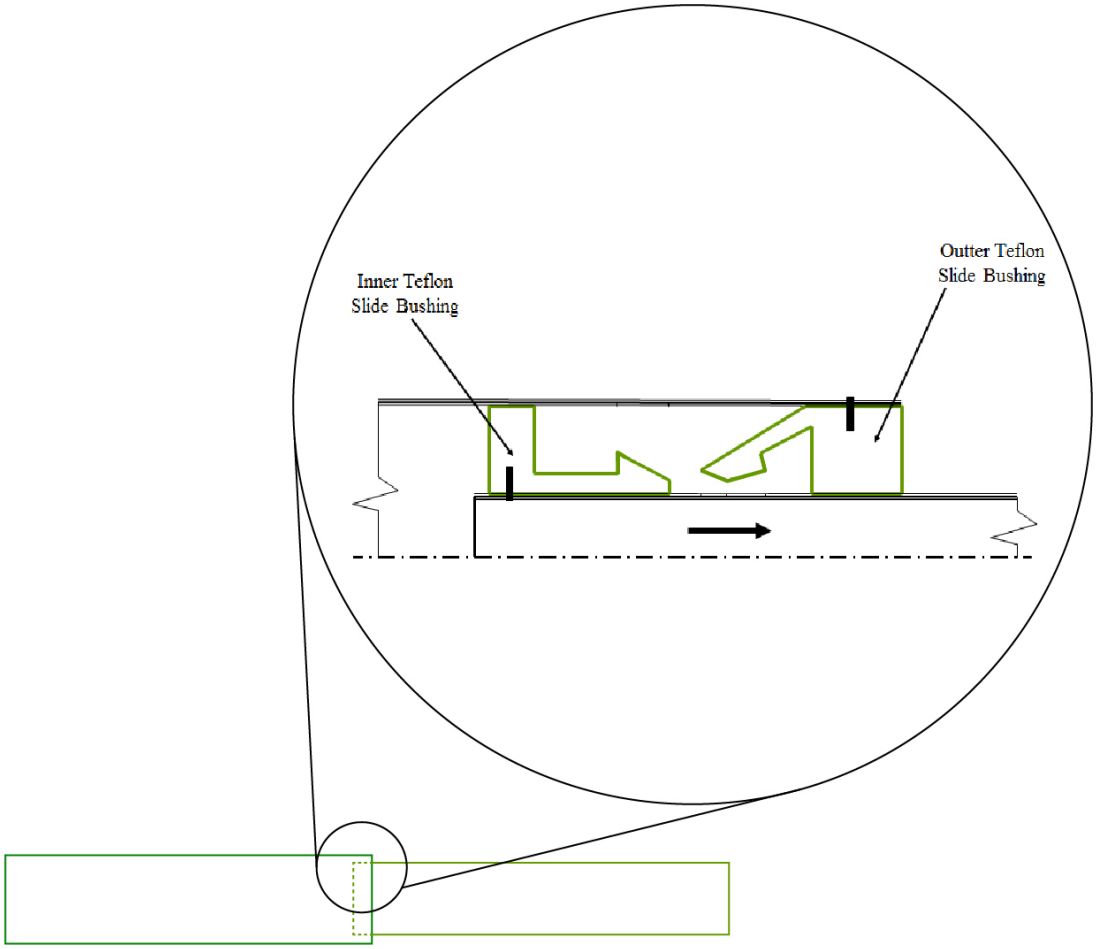

Figure 30: Boom slider and locking mechanism

Concerning the dimensions of the QuakeSat telescopic tubes, they were made of three segments each with a length of about 0.35 m and with the following diameters [34]:

- Segment 1 : Diameter = 38 mm
- Segment 2 : Diameter = 32 mm
- Segment 3 : Diameter = 25 mm

So the size of the tubes is comparable with that one selected for this study. The space between two consecutive tubes is about 6 mm or 7 mm, and for this study there is a similar gap between two elements. So the Teflon slides can be directly used with the same dimensions which are approximately of 2 mm high.

Figure 31: Latching mechanism

Then, concerning the latching mechanism, when a tube arrives at the end of its course it locks with the following, as represented in Figure 30. The CAD model of an inner telescopic tube with this latching mechanism is shown in Figure 32. The inner and the outer Teflon rings are visible.

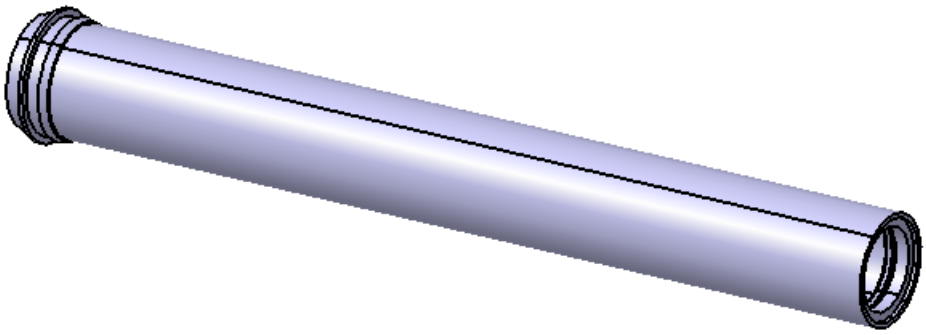

Figure 32: CAD model of latching mechanism

Finally there is no mechanism planned to retract the system, once the tubes are locked they stay in the same position. As part of this study it is not necessary, the telescopes have just to be deployed once and then kept in this configuration.

3.2.4 Kinematics of the deployment

The stowed configuration is shown in Figure 33, with the two telescopic booms and all the subsystems included in the design. The smallest internal tubes are fixed to the central CubeSat, while the largest external tubes are attached to the CubeSats 2U located on the both sides. The deployers are also included in the model.

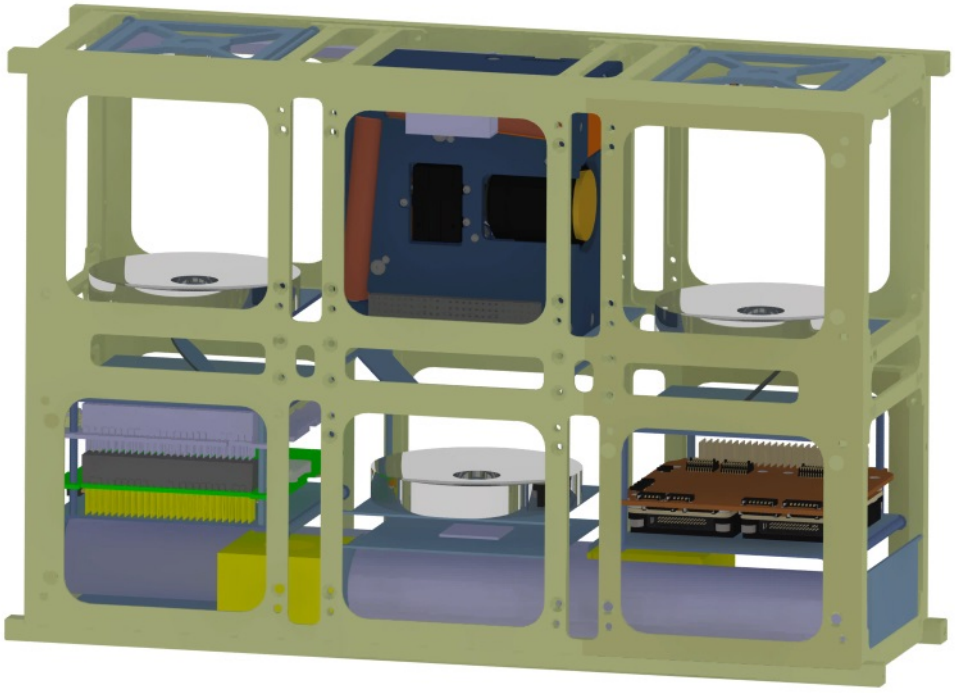

Figure 33: CAD model in the stowed configuration

During the first part of the deployment only the innermost tube is actuated by the motorization. So the two lateral CubeSats begins to be moved away from the central part. The tube is guided by the sliders in Teflon, until the lock joint of the smaller tube encounters the joint of the bigger tube and locks the two elements together. At that time, the smallest tube is in its maximal elongation, and is locked with the second tube. At this step, the configuration is the same as on Figure 34. The system is in its final configuration for the case where two elements compose the tubes. As it can be seen, the deployers stay fixed to the central CubeSat all along the deployment process.

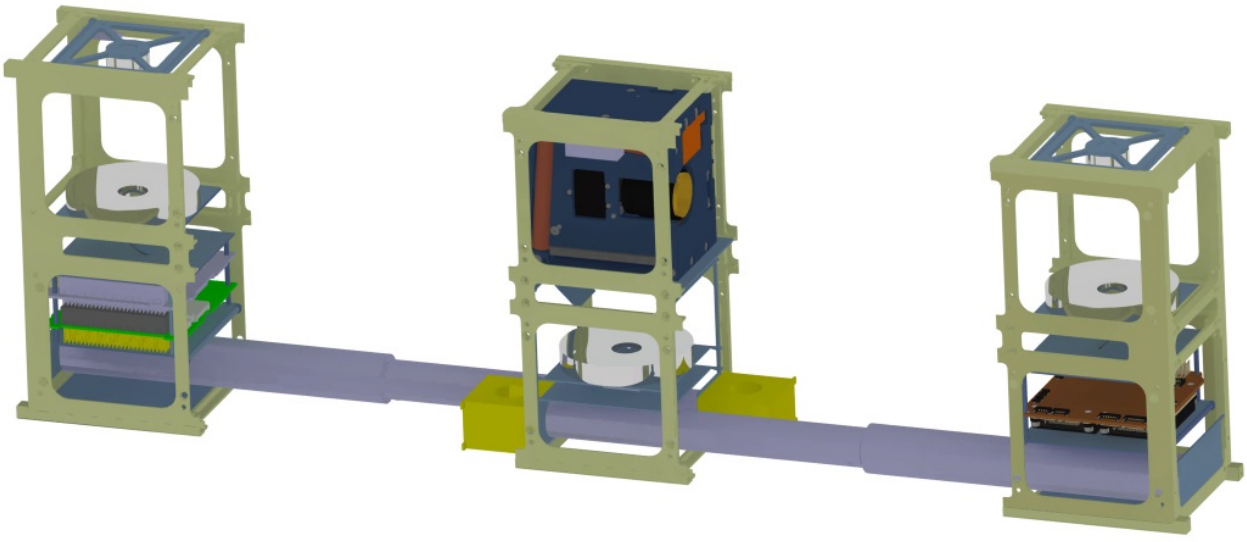

Figure 34: Deployment of the CubeSat - two tubes

If there is a third tube, the STEM actuator continues to push on the smallest tube, which is therefore moved further and drives the second tube. So the extension continues until the second tube latches with the external one. After that, the deployment is achieved and the CubeSats are in their final position, as represented in Figure 35.

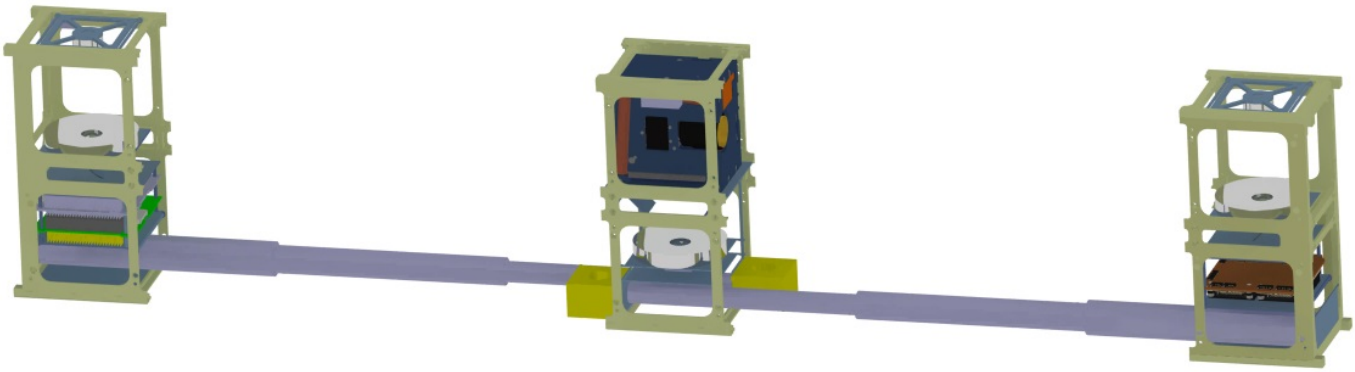

Figure 35: Deployment of the CubeSat - three tubes

3.2.5 Release mechanism

One of the operational requirement imposed to CubeSats 6U is that all deployables such as booms, antennas, and solar panels shall wait to deploy a minimum of 30 minutes after the CubeSat's deployment switches are activated during 6U Dispenser ejection. As the STEM actuator should have a passive deployment, a release mechanism has to be included, that maintains the system in the stowed configuration until the right time where it is deployed.

The *nichrome burn wire release mechanism* uses a nichrome burn wire that, when it is activated, heats up and cuts through a Vectran tie down cable allowing the deployable on the satellite to actuate. This release mechanism is shown in Figure 36 and utilizes a two saddle design with compression springs to apply a spring stroke and force to the nichrome wire to thermally cut the Vectran cable. So it is a low-cost, simple mechanism that is suitable for different deployables on a small satellite. It can be actuated with standard CubeSat bus power and has already been used successfully for a tether deployment. [35]

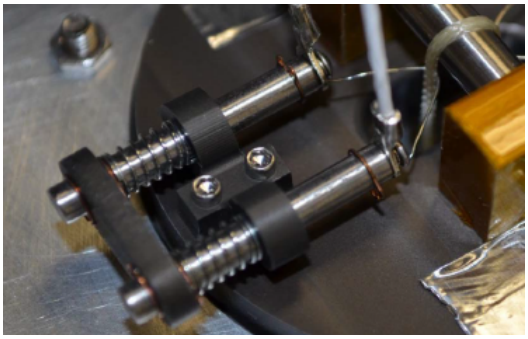

Figure 36: Nichrome burn wire release mechanism

3.2.6 Inclusion of guiding rails

As already explained, the stability of the deployed structure has a critical importance for the telescopes. They have to move as little as possible from their reference position. Indeed, the main difficulty of the optical aperture synthesis is the cophasing. To obtain a stable image, the paths travelled in the different arms of interferometry system have to be equalized. Actually, it is possible to use some correction tools that compensate the difference of path between the two telescopes but the structure has to be as rigid as possible. It is the reason why some elements can be added to the telescopic tube, in order to improve the rigidity.

Moreover, these other elements added can be used to prevent the rotation of the tubes. In this way, the relative weakness of the locking mechanism can be compensated so that the structure is completely locked once the boom extended.

A solution is to place guiding rails in the upper corners that will stiffen the structure. These elements can be also telescopic but with a rectangular section. By this way, they prevent largely the torsion of the tubes and the rotation of the deployed structure. It is preferable that these rails have a passive deployment, that they are not motorized but just driven by the telescopic boom movement. Hence, there is no problem of synchronization between the different deployable elements, and the guiding rails just accompany the CubeSat deployment if the applied force is sufficient.

If two rails are placed one against the other lengthwise, they can have each one an initial length of 150 mm. Then according to the number of tubes, they have to extend up to a length of about 300 mm or 500 mm.

When the main telescopic tubes are actuated, they move the lateral 2U and so the external rails follows the movement. However, they should not impede the deployment, so it must be verified that the force needed for their deployment corresponds to the force exerted by the STEM motorization. Moreover, a locking mechanism similar to the one of the telescopic tube has to lock the structure in the deployed configuration.

The best way to realize this is to imitate the design of the guiding and locking mechanism of the telescopic tubes. In this way, there is no problem of lubrication or tribology. Because this tubes are not motorized, it is necessary to apply a bigger force to deploy the telescopic boom, basically three times the value because three arms have to be deployed instead of one. Therefore, the guiding rails are easily extended and do not disturb the CubeSat deployment.

A force of 8.9 N was used to deploy the boom of QuakeSat. Thus here the telescopic tubes have to be pushed with a force of at least 26.7 N to correctly deploy also the guiding rails. This is far from the limitation of the STEM actuator, so a safety margin can be applied. Finally it is preferable that the actuator works with a force of 35 N.

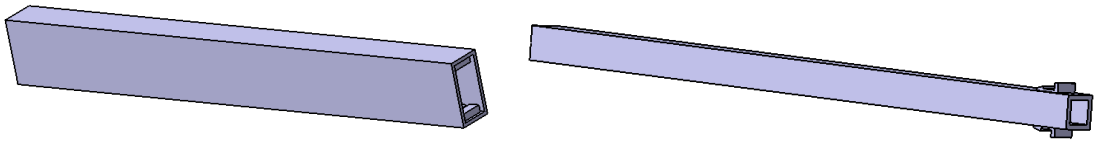

Figure 37: Internal and external rails

Furthermore, the rails should have the same number of elements as the number of tubes. If there are two tubes, two rails of 150 mm long are needed. They are represented in Figure 37. On the left, the external rail is visible with the slide in Teflon inside its surface. And on the right the inner rail is represented, with the slide bushing outside.

These sliding and locking parts in Teflon are detailed in Figure 38.

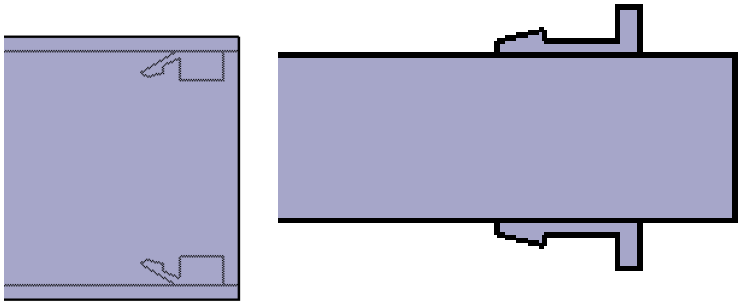

Figure 38: Detail of the sliding and locking mechanism

Concerning the dimensions, the rails have a section of 10 mm x 13 mm for the bigger one and of 7 mm x 7 mm for the smaller one. The slides are 2 mm high as for the telescopic boom, and are placed only on the top and bottom surface as it can be seen in Figure 39 where the right drawing details the section. The thickness is 1 mm and there is a gap of 0.5 mm between the sides of both rails. As it can be observed on Figure 39, there is enough space next to the ADCS to position the guides, which are placed on a support that is visible.

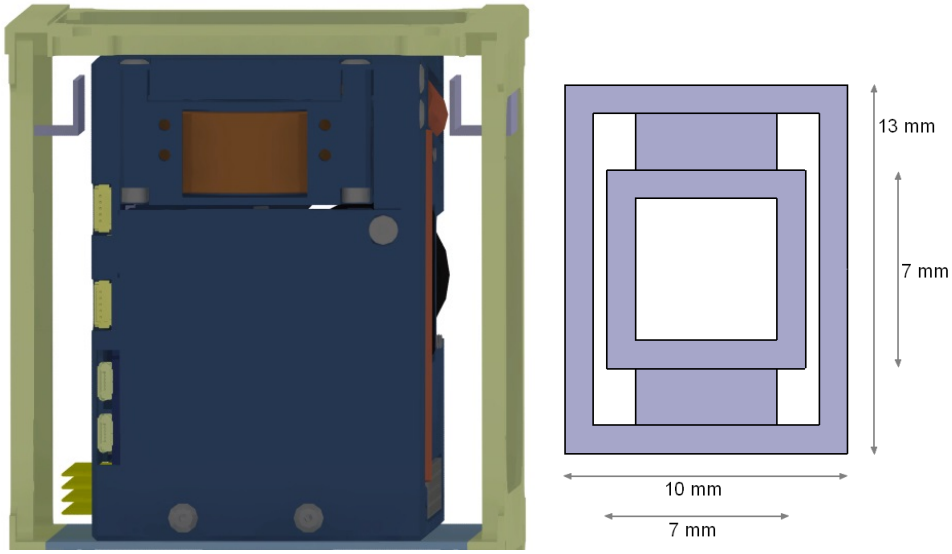

Figure 39: Position and section of the rails

The deployment with the guiding rails is shown in Figure 40. As it can be observed, the rails are perfectly inserted in the whole structure and do not disturb the incoming light on the telescopes.

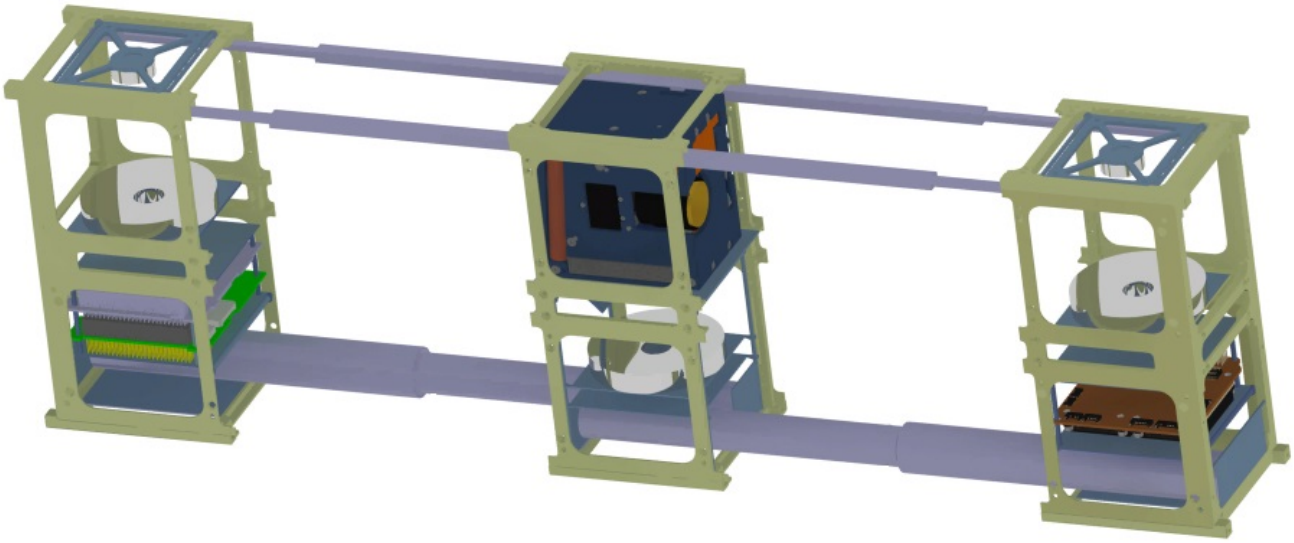

Figure 40: Deployment of the CubeSat with guiding rails

For the case where three tubes compose the telescopic boom, three rails have also to be used. As it can be seen in Figure 39, there is no place to increase the width of the section due to the ADCS but it is possible to increase the height of the rails. So if a third rail is placed inside the two others their height has to be increased so that the third rail has a section of 4 mm x 7 mm.

4 Modal Analysis

In order to study the rigidity of the structure, the normal modes of the deployed configuration are computed with the software *Samcef*. Indeed, the eigenfrequencies of a structure can be used to characterize its rigidity and its stability. This modal analysis is made for four different structures that are differentiated by the number of elements (two or three) forming the telescopic tubes, as well as by the presence or not of the guiding rails presented in the previous section.

For each of these cases, the first mode is represented here below. Then the ten first eigenfrequencies are listed in Table 4. The results obtained are compared to determine the influence of the tube length and of the support elements on the rigidity of the structure.

To get these results, the central CubeSat is considered as fixed, so the external faces of the inner tubes that are situated on the middle are clamped. Therefore the modal analysis represents the vibrations of the lateral CubeSat 2U once deployed. By clamping those faces, the rigid body modes are removed and only the mode shapes remain. But this is not the only way to proceed. Indeed, another possibility is to represent the whole spacecraft, without any face clamped and then to remove the rigid body modes. But this option was not retained.

Another important information is that the deformed structures shown in the next section are not depicting the exact reality. Indeed, the deformations are amplified to better represent the behavior of the satellite, the deformed structure is shown so that the major displacement corresponds to 10% of the major dimension of the structure. The value of the displacements induced by external disturbances is computed after.

The main CubeSat structure is made of aluminum 5052-H32 alloy. The telescopic tubes and guiding rails are also made of the same alloy for simplicity. The properties of this metal are the following, some of them will be useful for the thermal analysis :

- Density : 2680 kg/m^3
- Modulus of Elasticity : 70.3 GPa
- Poisson Ratio : 0.33
- Thermal Conductivity : 138 W/mK
- Thermal Expansion : 23.7e-6 K^{-1}

4.1 Comparison of the first mode shape

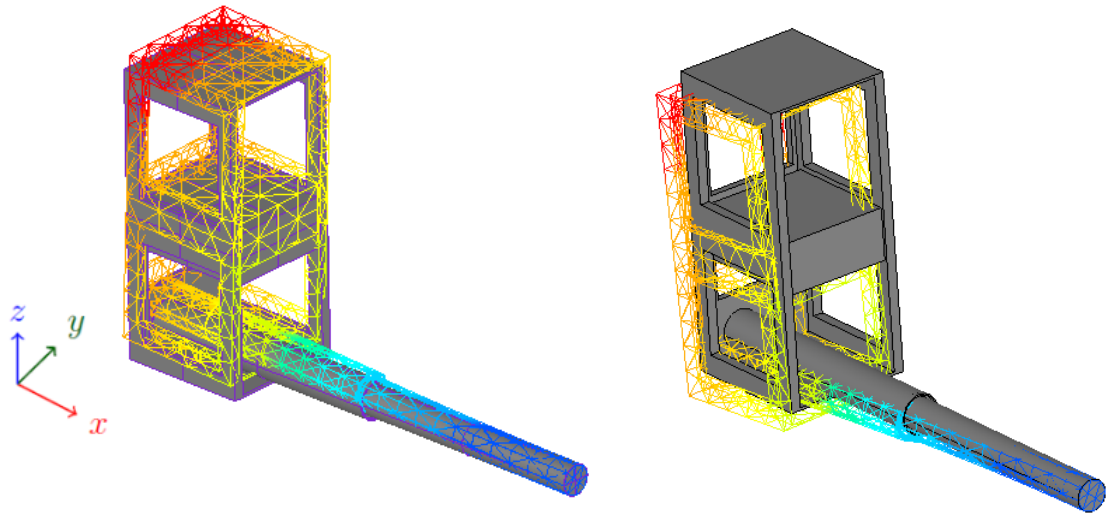

Figure 41: Modal analysis - Case 1

The first case consists in the structure with only two telescopic tubes and without guiding rails. The first mode shape corresponds to a bending in the vertical direction and the frequency associated with this mode is 26.99 Hz. However, the second mode shape happens at a frequency of 27.10 Hz, which is extremely close to the first one. This second mode corresponds to a lateral bending and is perpendicular to the first one. Actually both modes occur at the same frequency, the slight difference in their eigenvalue comes from some imprecision in the computations of *Samcef*. These two modes are represented in Figure 41. Therefore, if the satellite is excited around 27 Hz both modes will combine and the resulting displacements will be very important.

Concerning the reference frame, the three axes are represented on the figure and are valid everywhere, it is the same frame for all this work. So the vertical direction corresponds to the z axis, the direction of the tube is the x axis and the lateral direction is related to y. For the first mode, the biggest displacement occurs in the extremities of the CubeSat 2U, the upper part when the structure moves up as represented in the left figure. For the second mode shape, it can be observed that the lateral bending is accompanied by a small rotation of the structure. As explained before, the telescopic tube alone does not prevent the CubeSat from turning, which is the reason why the biggest displacements are situated also in the upper part of the structure.

Then, the second case studied is the same as the first one with just another tube added to the telescopic mast, as represented in Figure 42. The influence of this additional tube is studied by analyzing the difference on the eigenfrequencies. As expected, because the longer lever arm the frequency is lower for this case. The first mode shape is associated with a frequency of 16.17 Hz, and the second eigenfrequency is 16.36 Hz. So here again the same phenomenon happens with the two first mode shapes occurring at the same frequency and corresponding to perpendicular bending. The displacements of the structure are represented in Figure 42 and are the same as the previous case. Indeed, the mode shapes 1 and 2 are reversed from the case 1 but as explained they appear at the same frequency.

Regarding the value of the first eigenfrequency, there is a substantial difference with the previous case. This means that the structure will be excited easier, so for a lower frequency if the telescopic boom is composed of three tubes rather than two.

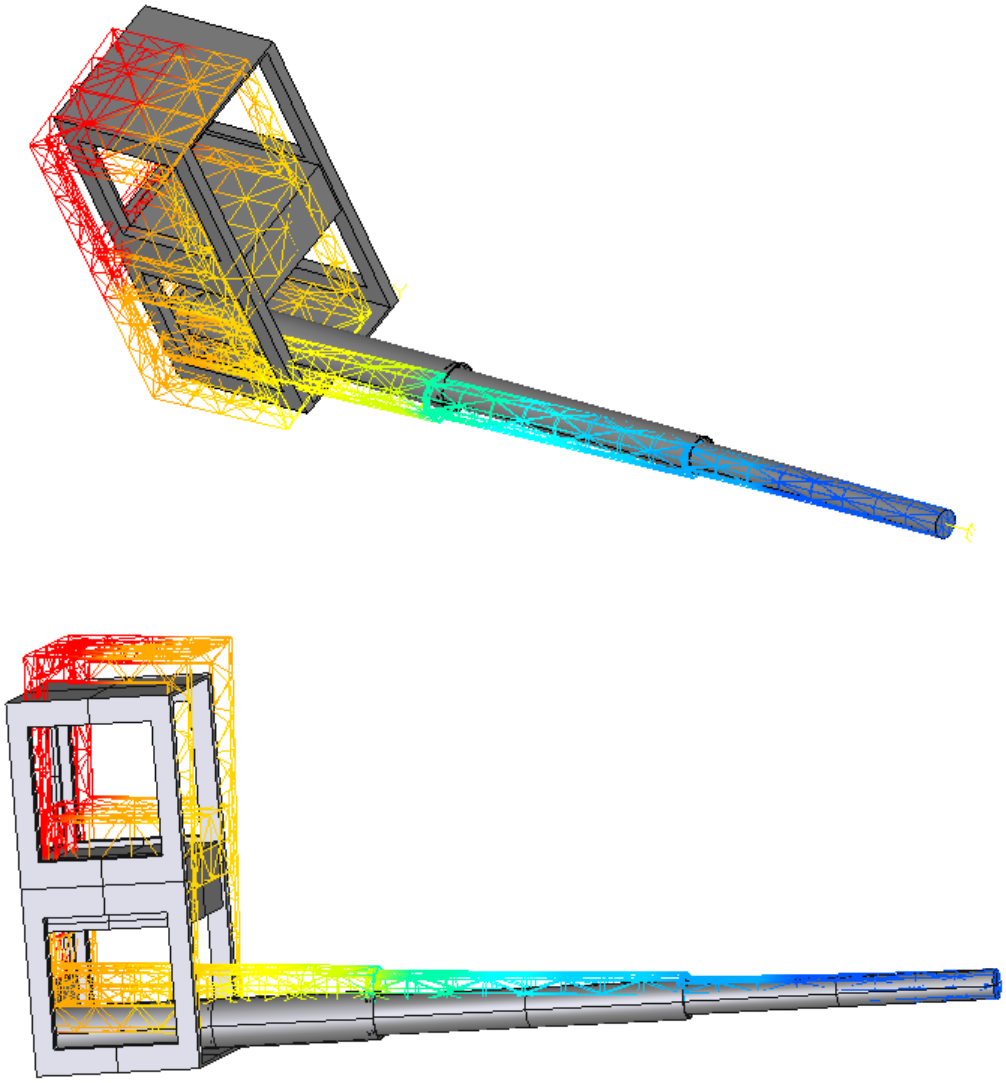

Figure 42: Modal analysis - Case 2

Actually, according to the specification required and the deployed length needed, one of these solutions (with two or three tubes) will be selected for a future application. Both have pros and cons. Indeed, a third tube allows to have a larger deployed structure, so a bigger apparent diameter and a better resolution. But in contrast the structure is excited at a lower frequency and the rigidity is weaker. Thus a compromise has to be found for the application in question.

For the third case guiding rails are added to the structure, and the telescopic mast has only two tubes like the first case. In the model built in *Samcef*, the extremity of the rails is also clamped. These elements give a better stability to the structure, which is reflected by the first eigenfrequency which is now 57.82 Hz. Moreover, the second mode shape occurs only at a frequency of 84.42 Hz. Thus add the rails involve at least two positive effects : the first mode happens at a frequency much higher and the two first modes are decoupled, they correspond to distant frequencies.

Here the spacecraft undergoes a bending in the lateral direction, the vertical bending happening at a higher frequency. However, the displacements differ from the case without guiding rails. Indeed, the biggest displacements are located on all the rear face and not just on the upper extremities. This is because the telescopic rails limit the rotation and thus the structure moves essentially laterally.

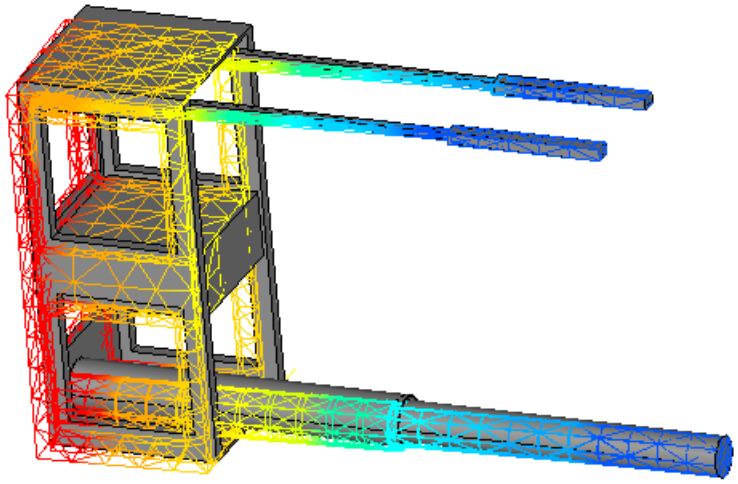

Figure 43: Modal analysis - Case 3

So the rails seem to be a good solution because it allows to improve the stability and to limit the displacements. For an equivalent telescopic tube length the value of the first eigenfrequency is more than doubled thus the guiding elements are very interesting.

Finally, the last case consists in the satellite with three tubes and guiding rails added. Here, the first mode appears at a frequency of 40.70 Hz, and is associated the same bending than the previous case as shown in Figure 44. In comparison with the case 2 which is the same structure without the supports added, this frequency is more than doubled. The conclusion is the same as for the previous case, guiding rails allow to increase the value of the first eigenfrequency and so to improve the rigidity and the stability of the deployed structure. They strengthen also the spacecraft so that the vertical bending is shifted and happen at an frequency much higher.

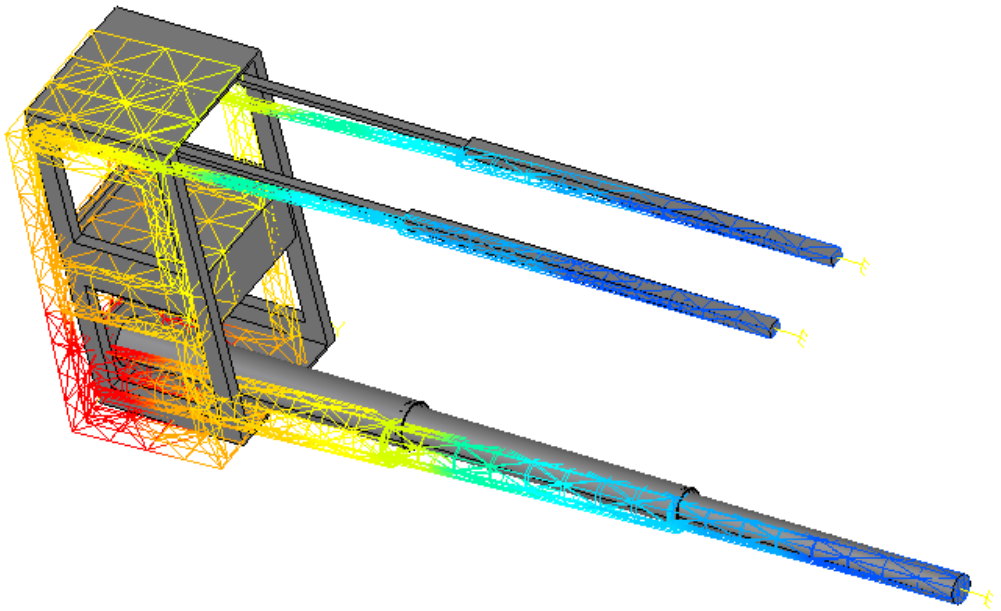

Figure 44: Modal analysis - Case 4

4.2 Comparison of the ten first mode shapes

Mode		1	2	3	4	5	6	7	8	9	10
Case 1	Frequency [Hz]	26.99	27.10	115.52	176.42	416.07	768.63	1496.68	1565.16	2095.90	2248.67
	Generalized mass [kg]	1.863	1.748	0.331	0.45	0.607	0.456	0.042	0.045	0.142	0.334
Case 2	Frequency [Hz]	16.17	16.36	91.04	154.14	340.48	590.32	1012.96	1070.71	2122.68	2131.95
	Generalized mass [kg]	1.186	1.436	0.350	0.445	0.24	0.425	0.047	0.045	0.045	0.047
Case 3	Frequency [Hz]	57.82	84.42	201.66	482.06	581.10	926.71	1508.35	1569.87	1908.20	2178.80
	Generalized mass [kg]	1.136	1.402	0.379	0.67	0.615	0.411	0.047	0.050	0.009	0.023
Case 4	Frequency [Hz]	40.70	59.23	172.37	424.36	504.01	705.99	997.01	1022.80	1114.66	1119.48
	Generalized mass [kg]	1.048	1.498	0.387	0.762	0.302	0.195	0.043	0.027	0.001	0.01

Table 4: Ten first eigenfrequencies and generalized mass for the four cases

In conclusion, this modal analysis proved that the addition of guiding rails is a relevant solution that improve the stability of the structure. Actually, the rigidity is represented by the values of the first shape modes of the structure which are set out in Table 4. From the rigidity point of view, the case 3 is the best choice because it corresponds to the highest value of the first frequencies. But the deployed length is lower than in the fourth case. So depending on the deployed length intended, one of these solution will be adopted.

By contrast, the same conclusion is no longer applicable for higher mode shapes. From the seventh mode, the case 2 has greater eigenfrequencies than the case 4. Likewise, from the ninth mode the case 1 has bigger frequencies than case 3. However to evaluate the rigidity of the structure, the first mode shapes are much more important than the others. The satellite will mainly be excited in the low frequencies and thus it is better that the first mode shape

corresponds to a higher frequency.

Finally the guiding rails have three major advantages : they increase the value of the first frequency, they decouple the two first mode shapes which reduce the displacements induced and they limit the rotation of the structure.

The generalized mass are also listed in Table 4 for each mode. It can be seen that they are much smaller from the seventh mode, because from the mode shapes 7 to 10 very little mass of the structure is set into motion.

Furthermore, here the modal analysis was carried out for the deployed structure and not for the unfold configuration. However, the modal frequencies of the satellite in its initial configuration have also to be computed in order to ensure that they are not coupled with those of the launcher. But this can be done in a further study, once the launcher will be selected.

Moreover, deeper modal, static and harmonic analyzes have to be performed to analyze that the entire structure survives during launch loads. Indeed, a satellite is submitted to different mechanical solicitations, namely variation accelerations, sine vibrations due to POGO phenomena, transient vibrations and random vibrations. Due to this dynamic environment to which satellites are confronted, different dynamic qualification tests are imposed. Here also these tests can be done in another study.

4.3 Harmonic response of the structure to an external acceleration

In this section, the response of the satellite to an harmonic acceleration is studied and the objective is to compute the displacements of the structure due to this perturbation and to determine what is the maximal acceptable value. The acceleration is applied to the entire body in a particular direction and the influence of that direction is studied. It has also a frequency range between 0 and 1500 Hz and a constant amplitude. The displacements of nodes A and B (see Figure 45) are computed, these nodes are located on the position of the primary and secondary mirror.

The goal is to determine the maximal amplitude that the acceleration can have so that the displacements of nodes A and B are limited to a maximum of 150 microns. According to the direction of the acceleration applied, different mode shapes participate to the deformation of the structure and the maximum displacements will occur at various frequencies with different magnitudes.

An acceleration applied on the entire volume is the most realistic representation of the disturbances that the spacecraft can undergo and represents effects of rotating unbalance due to reaction wheels or other actuators used to control the attitude of the satellite.

The guiding rails are included in the structure and once again two cases are compared, differentiated by the number of elements composing the telescopic boom. They correspond to case 3 and 4 of the previous analysis.

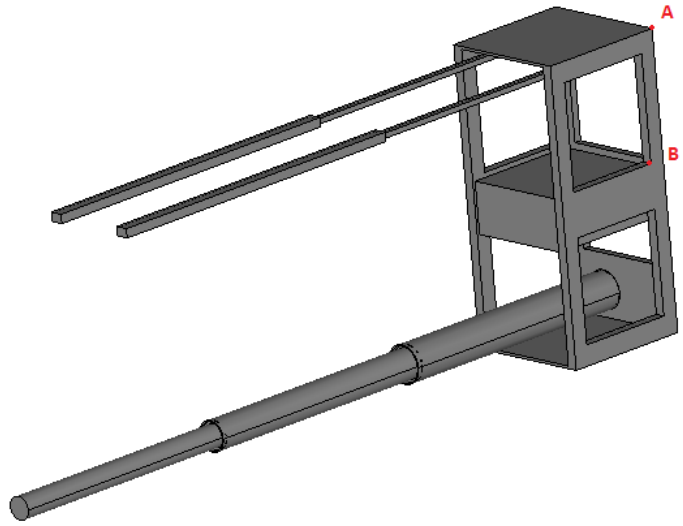

Figure 45: Nodes A and B

The computations are also made with the software *Samcef* with damping introduced in the model. Concerning the damping, it is one of the most important aspects to model and predict in structural analysis, as it determines for a major part the performances of a structural system or the amplitude of its vibrations. But it is also one of the most uncertain and difficult element to address in vibration analysis, due to the variety and complexity of its physical origin. A simple way to construct the damping matrix $\mathbf{C}$ that guarantees diagonal modal damping consists of making a weighted sum of the mass and stiffness matrices : [36]

$$\mathbf{C} = a\mathbf{K} + b\mathbf{M}$$

The matrix $\mathbf{C}$ obtained by this method is commonly known as *proportional damping* or *Rayleigh damping*. The modal damping ratios ϵ_r associated with the eigenfrequency ω_{0r}, are given by :

$$\epsilon_r = \frac{1}{2}(a\omega_{0r} + \frac{b}{\omega_{0r}})$$

In a first time, the hypothesis of a modal damping ratio close to 1% for the six first eigenfrequencies is made. In view of the higher mode shapes, it is not relevant to impose them a ratio. This is also confirmed by their much smaller generalized mass. These mode shapes are represented for the case 3 in Annex A and are equivalent for the case 4.

Actually, this method allows to compute the exact coefficients a and b for two modal damping ratios known. If the objective is to impose a ratio to more than two mode shapes, the system is undetermined and approximations have to be done. It is the case here and thus a least-square method is used to determine coefficients a and b such as the modal damping ratio of modes 1 to 6 are as close as possible to 1%. The resultant values for these coefficients are given here below, with the corresponding modal damping ratio.

$$\begin{cases} a = 3.372e-4 \\ b = 0.9186 \end{cases}$$

Mode	1	2	3	4	5	6	7	8	9	10
ϵ_r	1.20%	0.87%	0.56%	0.82%	0.94%	1.25%	1.73%	1.77%	1.92%	1.93%

Table 5: Modal ratios for 1%

As expected, the 6 first modes have a ratio around 1% and higher modes have a bigger ratio. In fact some modes are further than other from the nominal value, but a compromise must be done. The influence of the damping ratio on the displacements is determined in more details later.

In a first time, 10 modes are used to resolve the problem, the influence of the number of modes used is also studied later. The first structure analyzed is the case 4 presented previously.

To begin, an acceleration of 1g is applied in the z direction and the displacements obtained at nodes A and B are plotted as a function of the frequency. The graph represents the total movement undergone by the nodes, whatever the direction of this displacement.

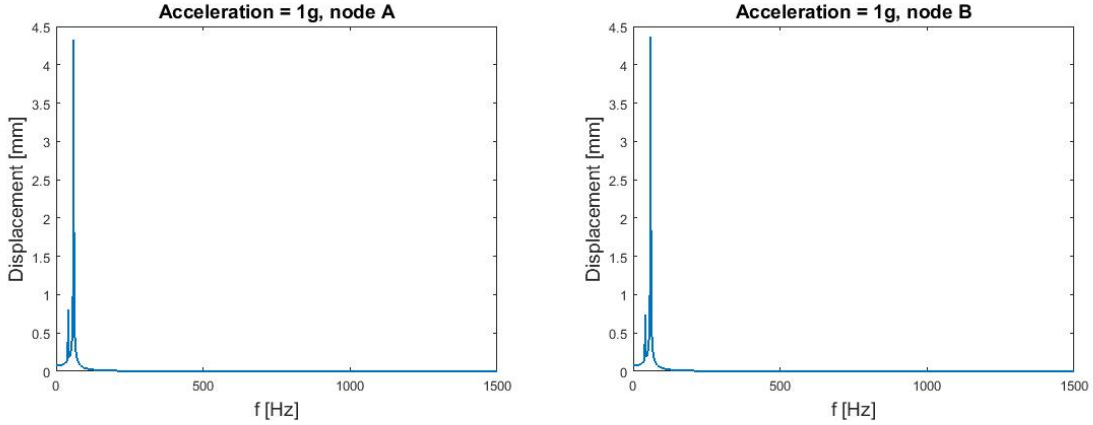

Figure 46: Displacements with an acceleration of 1g in the z direction

Both nodes have practically the same evolution. The maximum occurs at a frequency of 59 Hz and corresponds to a displacement of 4.324 mm for the node A and of 4.365 mm for the node B. This frequency corresponds to the second natural frequency of the structure computed before : 59.23 Hz, which is a bending in the vertical direction (see Annex A). However, contrary to what one may think, only two peaks are really visible and the displacement is almost zero for the rest of the frequency range. The second peak appears before, at a frequency of 41 Hz which corresponds to the first mode shape (40.70 Hz). But this peak is much lower than the second one because the mode shape associated is a bending in the lateral direction.

Actually for most of the natural frequencies, especially for the last four modes, the perturbation of the structure in the vertical direction do not lead to displacements of nodes A or B. In addition, other modes correspond to torsion and so the magnitude of the total displacement is less than for bending. To illustrate this, the ten first mode shapes of the case 3 are represented in the Annex A). And finally, other modes are activated for an acceleration in another direction, which will be illustrated later.

Then, the intensity of the external acceleration is divided by ten, and the corresponding displacements are shown in Figure 47.

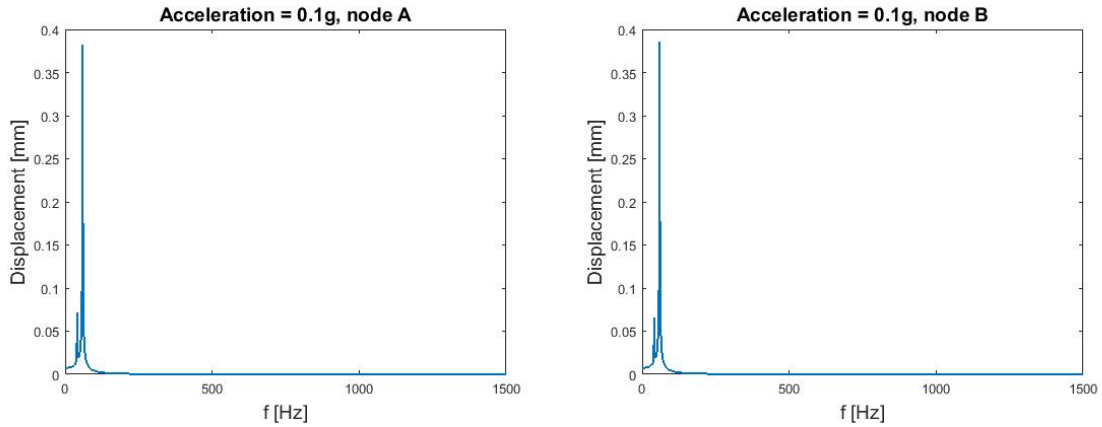

Figure 47: Displacements with an acceleration of 0.1 g

As expected, because of the linearity of the system, the graphs obtained are exactly the same as for an acceleration of 1g with the value of the displacements ten times lower. So trivially, it can be concluded that a maximal acceleration of 0.035 g applied on node A can be allowed in order to have a displacement lower than 150 microns, if this acceleration is applied with a frequency around 59 Hz, in the z direction. This corresponds to an acceleration of 0.340 m/s^2.

4.3.1 Influence of the damping ratio

As already explained, damping was included in the model to represent the energy dissipation that is always present in structural dynamics and in real structures.

Previously, the results were obtained with a ratio of approximately 1% for the six first mode shape. This was an assumption and in practice the modal ratios should be determined by experimental results to confirm the simulations.

By now, the coefficients a and b are computed to have approximately damping ratios of the order of 2% for the first six modes. The values obtained for the modal ratios are given in Table 6, with the following values for the coefficients a and b.

$$\begin{cases} a = 6744e-7 \\ b = 1.837 \end{cases}$$

Mode	1	2	3	4	5	6	7	8	9	10
ϵ_r	2.39%	1.75%	1..11%	1.65%	1.88%	2.51%	3.45%	3.54%	3.84%	3.86%

Table 6: Modal ratios for 2%

Here, the damping ratio are increased for each mode. And as before the six first modes have a damping around the expected value.

Then, the comparison between the displacements obtained for these values and those computed previously is represented in Figure 48.

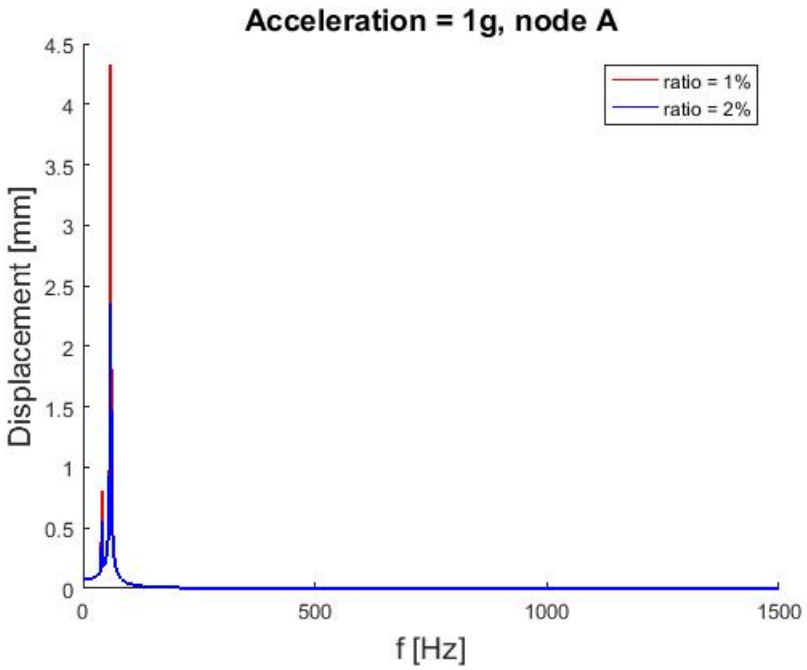

Figure 48: Comparison of the displacements with two different ratios

Multiply the damping ratio by a factor two decreases the displacement at the natural frequencies. The more the structure is damped, the lower the displacements are. Here, for a ratio of 2%, the node A has a displacement of 2.358 mm which is almost half of what is obtained with a damping of 1%. So if the structure has a higher damping ratio, the maximal acceleration allowed is increased.

4.3.2 Influence of the number of modes

To resolve the problem the software *Samcef* uses a modal superposition method, commonly used to solve the equations of motion of a system submitted to external forces. For a structure of n degrees of freedom the response can be written through modal expansion :

$$q(t) = \sum_{s=1}^{n} \eta_s(t) x_s$$

But in practice all modes cannot be computed or it would take too much time, so the solution is built with a limited number of modes. If only k modes are used, the modal expansion is restricted to :

$$q(t) = \sum_{s=1}^{k} \eta_s(t) x_s$$

For the results obtained before, only ten mode shapes were considered. Figure 49 compares the solutions calculated different number of mode shapes, in order to see if there are differences.

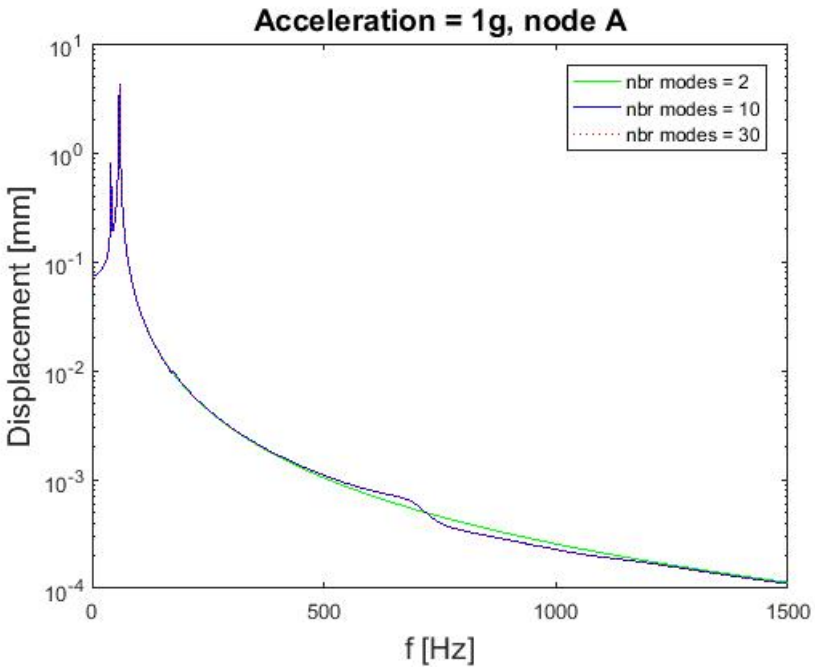

Figure 49: Comparison of the displacements with different number of modes

The graph is plotted for 2, 10 and 30 mode shapes with a logarithmic scale for the displacements. This is done for several reasons.

First, it highlights the small differences between the three curves. These differences happen after 500 Hz, when the modes beyond the second one have a slight influence. Then it demonstrates that a perturbation below 1500 Hz in the vertical direction will generate displacements only at the two first mode shapes. Indeed, for the rest of the frequency range the structure is practically not excited and only tiny variations are registered after the second peak.

Therefore, two modes are already sufficient to represent correctly the movement of the structure in the case of such an acceleration. And as expected there is no difference between 10 and 30 modes because the eigenfrequencies after the tenth are out of the frequency range of the applied acceleration. However, it is necessary to use more than two modes for accelerations in other directions than along z axis because they will activate other modes.

4.3.3 Comparison with case 3

Until now, the displacements have been obtained with the geometry configuration wher three tubes compose the boom. Here, they are computed for the case 3 : guiding rails and two tubes instead of three for the telescopic tube. The same analysis is made, an acceleration of a magnitude of 1g is applied vertically to the body and the displacements according to the frequency of this acceleration are plotted in Figure 50. Ten modes are used for the calculation and a modal damping of 1% is used.

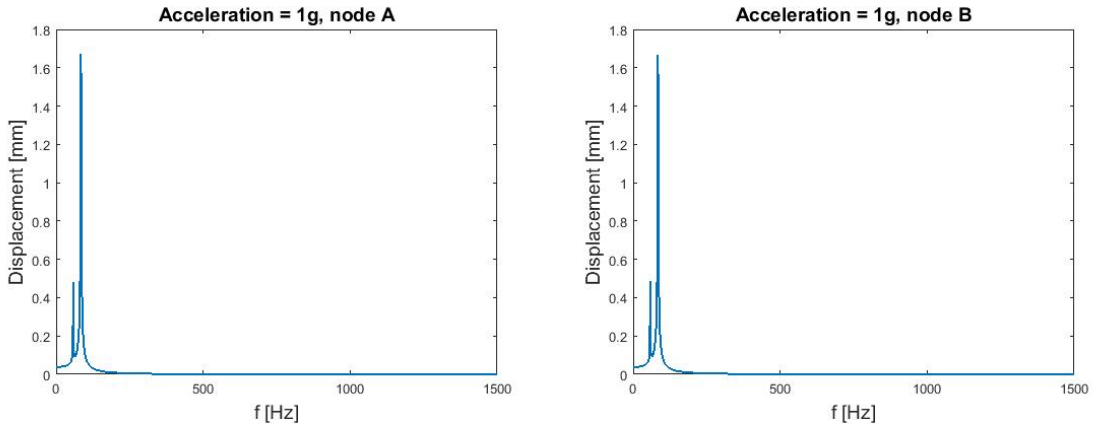

Figure 50: Displacements of the nodes for the case 3

The graphs look the same as for the case 4 : two peaks are visible, a first one smaller corresponding to the first mode shape (here 57.82 Hz) and the second peak higher, linked with the second eigenfrequency (84.42 Hz). Here again, the nodes A and B undergo almost the same displacement, which has a maximal value about 1.671 mm for node A and 1.664 mm for node B. So because the same relationship between force applied and displacement exists, the maximal force allowed to limit the movement of mirrors at 150 microns is now 0.09 g, in other words 0.881 m/s^2.

4.3.4 Influence of the direction

So far, all the accelerations have been applied only in one direction : vertically along the z axis. Figure 51 represents the graphs of the displacement obtained at node A for an acceleration of 1g in the x and y directions.

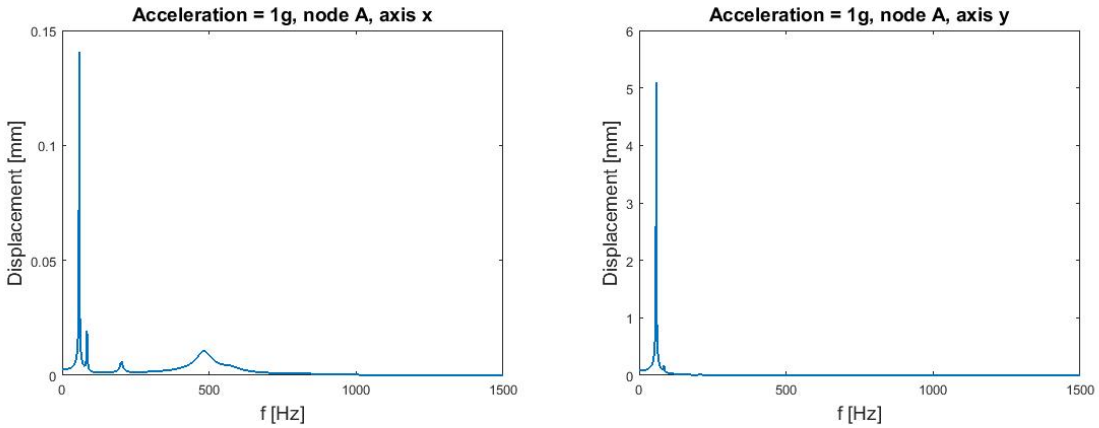

Figure 51: Displacements in x and y direction

On the graph on the right, corresponding to an acceleration in the y direction, only one peak is visible at the first eigenfrequency, which corresponds to a lateral bending. Here the displacements are greater than for an acceleration in the vertical direction. But for the rest of the frequency range, the structure is almost not disturbed.

In contrast, an acceleration in the x direction induces displacements for several frequencies. The bigger peak appears still at the first frequency, but other variations correspond to the second, third and fourth mode shapes. However, the order of magnitude of the vibrations is much lower for an acceleration in this direction compared with the others.

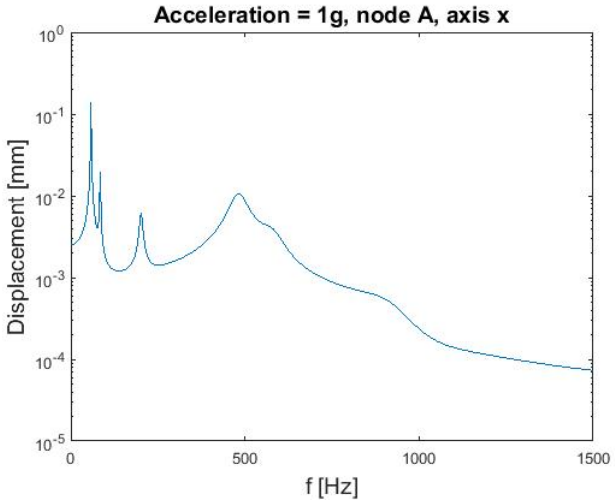

Figure 52: Displacements in x direction - logarithmic scale

It is interesting to use here also a logarithmic scale to study the response of the structure to an acceleration in the x direction. Indeed, six peaks can be seen in Figure 52 which corresponds to the six frequencies under 1500 Hz. The greater movement of the structure still happens at the second peak but the graph shows that the nodes A undergoes a displacement at each eigenfrequency.

Table 7 summarizes the displacements of the node A for an acceleration of 1g applied in each direction. Only the maximum displacement is written with the frequency at which it happens.

	Case 3		Case 4	
	Frequency [Hz]	Displacement [mm]	Frequency [Hz]	Displacement [mm]
x	58	0.146	41	0.165
y	58	5.091	41	8.14
z	84	1.671	59	4.324

Table 7: Maximal displacement for 1g in each direction

A few remarks about the results. First, for a same case the maximum displacements occur at the first mode shape of the structure for a perturbation in the lateral direction. Thus the movement of the body is the most important for an acceleration imposed in the y direction and the less important in the x direction. In any case, the maximal displacement occurs at the first or the second eigenfrequency which are useful to determine the rigidity of the structure.

Then use a shorter boom length allows to increase the value of this critical frequency and to reduce the displacement caused. Therefore, reduce the deployed length increases the

rigidity of the spacecraft, as it was expected.

Hence, the disturbance resulting in a displacement of 150 microns is different according the direction of application. The corresponding values are noticed in the following table, which resumes the specifications of the CubeSat.

	Case 3		Case 4	
	Frequency [Hz]	Acceleration allowed	Frequency [Hz]	Acceleration allowed
x	58	1.027 g = 10.079 m/s^2	41	0.909 g = 8.918 m/s^2
y	58	0.029 g = 0.289 m/s^2	41	0.018 g = 0.181 m/s^2
z	84	0.09 g = 0.881 m/s^2	59	0.035 g = 0.340 m/s^2

Table 8: Maximal accelerations allowed

Concerning the rest of the frequency range, in view of the graphs shown previously, it can be concluded that there is no limit for the acceleration allowed. Indeed, the accelerations that the CubeSat will undergo in practice will induce very limited displacements of the structure outside the peaks mentioned in Table 8.

Finally, this analysis showed the differences between a telescopic boom composed of two and three tubes. For the first case, a displacement of 150 microns is achieved for an acceleration of higher magnitude and at a higher frequency compared with the second case. Therefore, this configuration presents a higher stability and undergoes less important displacements for a same acceleration than the other one. So, if two tubes are long enough to achieve a sufficient resolution for the telescopes, this solution will be retained.

Furthermore, it is important to note that accelerations with a magnitude higher than 1g can be applied to the structure without generating displacement greater than 150 microns, if the frequency of these accelerations does not correspond to the eigenfrequencies of the structure. So here the worst case was considered to compute the maximal perturbation allowed.

5 Thermal analysis

Another important analysis that has to be done before starting a space mission is the study of the different temperatures that the satellite is facing. For this work, it is also really important to evaluate approximately the difference of temperature between the extremities of the spacecraft, so the two external CubeSats 2U and the central part. Indeed, if there is a difference of temperature the boom will extend or shrink and the mirrors will no longer be accurately positioned.

5.1 Details of the analysis

The satellite is assumed to be in a sun-synchronous orbit at an altitude of 600 km, which is usual for observations. The goal is to evaluate the elongation of the booms induced by a difference of temperature between the central CubeSat and the external units, in order to see if this can be compensated by an actuator placed on the mirror.

Two different cases are studied, represented in Figure 53, corresponding to particular position of the spacecraft along its orbit where there are differences of temperature between the three CubeSats.

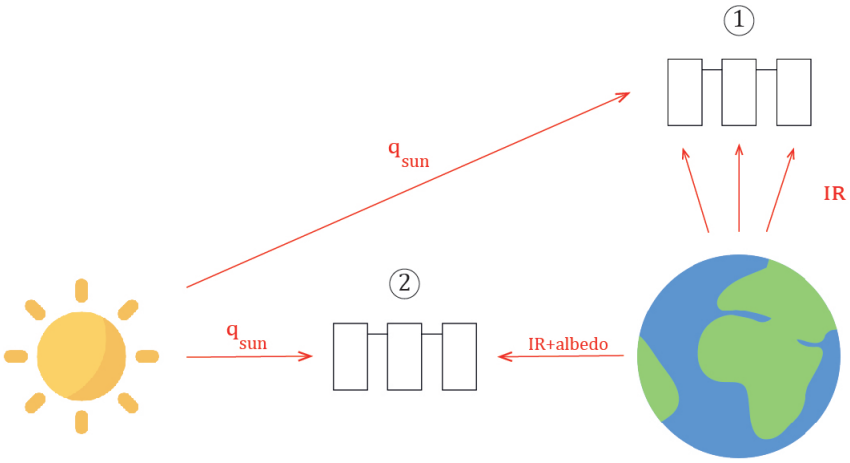

Figure 53: Cases studied

The spacecraft is represented by a very simple model. One node is placed in the middle of each CubeSat 2U and resumes the fluxes coming on the 6 faces around. It is a uni-dimensional study, so once the temperature of one node computed, all the corresponding CubeSat 2U is assumed to be at the same temperature. So that finally three temperatures are obtained, one for each CubeSat and there is a longitudinal gradient of temperature along the direction of the boom.

A fourth node represents the deep space which has a temperature $T_4 = 4\text{K}$. Between the node 2 placed in the center of the satellite and the nodes 1 and 3 placed in the middle of the external CubeSats there are exchanges by radiation and by conduction through the telescoping boom. And each node emits also by radiation towards the deep space. Finally, using the electrical analogy, the equivalent thermal circuit is represented in Figure 54.

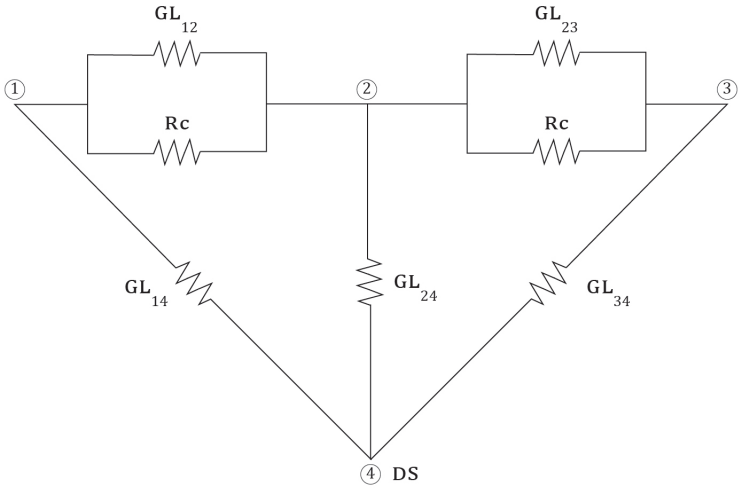

Figure 54: Thermal circuit

There are three principal forms of environmental heating that reach the faces of the body. The first one q_{sun} is directly coming from the Sun, and the two others come from the Earth : q_{IR}, the infrared emission of the planet, and q_{albedo}, the reflection of the sunlight on the surface of the Earth. The expression of these fluxes is the following :

$$\begin{cases} q_{sun} = F_{sun}A \\ q_{IR} = \sigma T_{Earth}^4 F_{Earth} \epsilon A \\ q_{albedo} = a F_{sun} cos(\theta) F_{Earth} A \end{cases}$$

A lot of symbols appear in these expressions and here are their meanings :

- F_{sun} is the solar flux, which varies over year and is on average : 1367.5 W/m^2,
- A is the area of the CubeSat face,
- σ is the Stefan-Boltzmann constant : 5.67e-8 $Wm^{-2}K^{-4}$,
- T_{Earth} is the temperature of the Earth and is on average : 247.27 K,
- F_{Earth} is the view factor between the spacecraft and the Earth, for a plate facing the Earth it can be approximated by : $\frac{R_{Earth}}{R_{orbit}^2}$,
- a is the albedo and is on average 0.38,
- θ is the angle between the solar vector and the position of the spacecraft (see fig. 55).

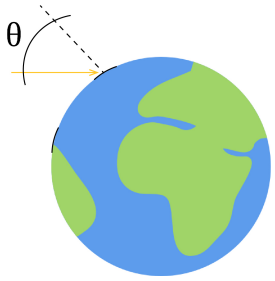

Figure 55: θ angle

Actually, the intensity of the albedo will vary with the angle θ, and will be maximal when θ is equal to zero so when the satellite is in the position 2 of Figure 53. And the albedo flux will be zero when the spacecraft is in the position 1. So if the observations are made during the half-period, between θ equals to 90°to -90°when the satellite faces the Sun, the sunlight and the infrared emission from the Earth can be considered as constant with only the albedo varying. So the cases 1 and 2 represent the moment when the flux is maximal and minimal during the observations.

Then, concerning the resistances present on Figure 54, there are two kind of them : GL the thermal conductance and GR_{ij} the radiative exchange factor. Their expression is given by :

$$\begin{cases} GL = \frac{kS}{l} \\ GR_{ij} = \epsilon A B_{ij} \end{cases}$$

where

- l is the length of the telescoping boom : 0.4 m for two tubes and 0.6 m for three,
- k is the thermal conductivity of Aluminium : 138 W/mK,
- S is the section of the boom,
- ϵ is the emissivity of the Spacecraft : 0.8,
- B_{ij} are the Gebhart factor between surface i and j.

Concerning the thermal conductivity, k varies with temperature but this variation can be neglected if the range of temperature is typically comprised between 0°C 200°C. So here a constant value is taken and this hypothesis is verified by checking the temperatures obtained.

The Gebhart factors represent the fraction of radiation emitted by an isothermal surface A_i that reaches another surface A_j directly or after multiple reflections with other surfaces A_k. They depend on the emissivity ϵ, the reflection ρ given by 1-ϵ and by the view factors, which are given in the next table.

To compute the view factors, only one formula is needed and is given in Annex B : the expression of the view factor between two parallel rectangles. Then, from the relationship $\sum_{j=1}^{4} F_{ij} = 1$ all the other view factors between nodes can be computed. The value of F_{Earth} is also given in the Table.

	F_{12}	F_{13}	F_{14}	F_{23}	F_{24}	F_{34}	F_{Earth}
Two tubes	0.1167	0	0.8833	0.1167	0.7667	0.8833	0.9122
Three tubes	0.0362	0	0.9638	0.0362	0.9276	0.9638	0.9122

Table 9: View factors

A few remarks about this table. First all the view factors are not written, indeed F_{ii} is equal to zero and the reciprocity relation gives $F_{ij} = F_{ji}$. Then because of the symmetry of the problem, the same value is computed for F_{14} and F_{34}. F_{24} is lower because the spacecraft placed in the middle sees the two other CubeSats and thus exchange less flux with the deep space.

Otherwise, the CubeSat 1 does not exchange heat by radiation with the CubeSat 3 and thus $F_{13} = 0$. Finally, the view factors between the nodes 1 to 3 and the deep space are the highest for each node. They are also bigger for a longer telescopic tube because the surfaces of the satellites are separated by a higher distance.

Now, it remains to write the equations of the thermal equilibrium at each node. For the first case represented in Figure 53, each node of the spacecraft receive a flux from the Earth. But this contribution comes only from the infrared emission and not from the albedo because the angle θ is about 90°. In addition the solar flux impacts the node 1. So the equations to solve in order to get the temperatures T_1, T_2 and T_3 are the following.

$$\begin{cases} q_{sun} + q_{IR} + \sigma G R_{12}(T_2^4 - T_1^4) + \sigma G R_{14}(T_4^4 - T_1^4) + GL(T_2 - T_1) = 0 \\ q_{IR} + GL(T_1 - T_2) + \sigma G R_{12}(T_1^4 - T_2^4) + \sigma G R_{24}(T_4^4 - T_2^4) + \sigma G R_{23}(T_3^4 - T_2^4) + GL(T_3 - T_2) = 0 \\ q_{IR} + GL(T_2 - T_3) + \sigma G R_{23}(T_2^4 - T_3^4) + \sigma G R_{34}(T_4^4 - T_3^4) = 0 \end{cases}$$

There are three equations and three unknowns T_1, T_2 and T_3 with $T_4 = 4$K. So this non linear system can be solved with a non linear solver such as the $Maltab$ function $fsolve$.

5.2 Results

The temperatures obtained for the case where the boom is composed of two and of three tubes are given in Table 10. To compute the elongation of the booms the difference of temperature is taken between their initial length at 20°C and their mean temperature in orbit. This value is given by the average between the temperatures of the two extremities which are computed. So the elongation is given by :

$$\Delta_L = \alpha(T_{mean} - 20)L_0$$

Where α is the diffraction coefficient of aluminium which is 23e-6 K^{-1}, L_0 the temperature at 20°C and T_{mean} the average between the temperatures computed at the extremities of the boom for each case.

	Two tubes	Three tubes
T_1 [°C]	78.810	71.203
T_2 [°C]	77.278	68.564
T_3 [°C]	76.461	67.232
Elongation 1 [mm]	0.785	1.102
Elongation 2 [mm]	0.801	1.147
Difference [mm]	0.016	0.045

Table 10: Temperatures for the case 1

As expected, for each node the temperature is higher for a shorter tube because if the length of the boom is increased the thermal conductance is lower and thus the gradient of temperature between two faces of the CubeSat is greater. Because of this, the elongation is more important for a three tubes boom. The elongation 1 corresponds to the elongation of the tube placed between nodes 1 and 2 while elongation 2 corresponds to the other boom. What is important is the difference between these elongations, if both booms have the same extension it is not a problem since the paths between the mirrors and the detector remain the same.

Here this difference is about 16 microns for two tubes and about 45 for three tubes. So it is not negligible for the accuracy of the mirror positioning.

Obviously, the highest temperature is T_1, which faces the Sun. And the difference of temperature is bigger between the nodes 1 and 2, than between 2 and 3, so one boom will extend more than the other.

Then for the second case, there is only the node 3 which receive a flux from the Earth, given by the infrared and the albedo. And the node 1 still receive the light from the Sun. So the equations become :

$$\begin{cases} q_{sun} + \sigma GR_{12}(T_2^4 - T_1^4) + \sigma GR_{14}(T_4^4 - T_1^4) + GL(T_2 - T_1) = 0 \\ GL(T_1 - T_2) + \sigma GR_{12}(T_1^4 - T_2^4) + \sigma GR_{24}(T_4^4 - T_2^4) + \sigma GR_{23}(T_3^4 - T_2^4) + GL(T_3 - T_2) = 0 \\ q_{IR} + q_{albedo} + GL(T_2 - T_3) + \sigma GR_{23}(T_2^4 - T_3^4) + \sigma GR_{34}(T_4^4 - T_3^4) = 0 \end{cases}$$

And the temperatures computed for this case are set out in Table 11.

	Two tubes	Three tubes
T_1 [°C]	85.542	77.445
T_2 [°C]	84.342	75.7367
T_3 [°C]	84.184	75.153
Elongation 1 [mm]	0.896	1.297
Elongation 2 [mm]	0.887	1.271
Difference [mm]	0.009	0.026

Table 11: Temperatures for the case 2

Observing this table, the same remarks about the evolution of the temperature can be done, with still T_1 the highest temperature. Here the temperature gradient is smaller and the case 4 has still a difference of elongation three times more important than the case 3. So the solution with two tubes presents again the advantage of a shorter lengthening. Globally,

the temperatures are higher because the heating from albedo is here maximal with an angle θ of 0°.

	Flux - Node 1	
	2 tubes	3 tubes
Conduction to node 2	-0.1759 W	-0.1778 W
Radiation to node 2	-0.0002 W	-0.0001 W
Radiation to node DS	-0.1283 W	-0.1265 W
Solar flux	0.2735 W	
Infrared flux	0.0309 W	
TOTAL	0 W	0 W

Table 12: Exchange fluxes for the node 1 - Case 1

From Table 12, it becomes apparent that the conduction is much more important than the radiation for the heat exchanges between two parts of the satellite. The radiation is actually really low because the view factor between the surfaces is very small : 0.1167 if there are two tubes and only 0.0362 if there are three tubes. So to decrease elongation of the telescopic tubes, it is necessary to reduce the gradient of temperature between two CubeSats 2U, and the best way to achieve this is to minimize the transfer by conduction. Then, the thermal equilibrium is checked because the sum of the different fluxes coming in and out of the node 1 is equal to zero.

Throughout its orbit, the satellite is in the shadow of the Earth during a period at which it does not receive any flux from the Sun. But this case is not studied because the observations cannot be done during eclipse, so even if the booms extend it has no influence on the measurements. Indeed, a CubeSat has not so much own inherent power, and can only make observations when it sees the Sun, thanks to the power from the solar panels.

This thermal analysis was made with some assumptions, and with a very simple model. To represent exactly all the heat transfers between and inside the CubeSats, a much deeper analysis is needed. All the components have to be taken into account, their performance studied as wall as their impact on the surroundings. However, for a preliminary study the important is to know the order of magnitude of the temperatures that the satellite will have along its orbit, and the gradient that can appear between the different parts. This first computation of the differences of temperatures that can occur between the extremities of the deployable structure was interesting and showed that the elongation of the telescoping boom could not be neglected. Indeed, according to the results, during the observations the elongation varies between 30 and 90 microns and has to be compensated.

6 Optics

As explained before, the main difficulty of the optical aperture synthesis is the cophasing. The paths travelled by the light in the two different arms of the system have to be equalized. Indeed, to combine correctly the two beams coming from telescopes, the optical path difference between signals has to be lower than the wavelength observed.

Actually, it is possible to use some correction tools that compensate the difference of path between the two telescopes. The nature of the tools selected for depends on the range of length that has to be covered. Previously, the deployment of the telescopic tubes was assumed to have an accuracy of about 0.1 mm. And the modal analysis determined the maximal accelerations allowed that lead to a displacement of 150 microns. So a device able to compensate a hundred of microns is requested.

6.1 Telescope positioning adjustment

First it is necessary to adapt the position of the mirrors once the structure deployed. So a device is needed that can induce displacement in one direction, the longitudinal one : x. This device need to be used just once, after the deployment of the CubeSat.

Piezoelectric actuators are typical materials that can be used for this kind of application. They can be direct or amplified. For a direct actuator, the travel path is limited and generally does not exceed 100 μm while an amplified can travel up to 500 microns. They have to be fixed to a travel stage to control precisely the motion of the mirror. For this work, they are fixed to the mirrors inclined at 45°and thus situated in the central CubeSat.

The NPM140 Piezoelectric Micrometer Adapter provides nanometer positioning capability for manual products. A coarse adjustment is done with the manual screw and the final and fine adjustment is accomplished by controlling the piezo voltage of the device. It is an actuator built by *Newport* that may be suitable. It is represented in Figure 56 and its main characteristics are given in Table 13. [37]

Figure 56: Piezoelectric actuators from *Newport*

	Travel range	Resolution
NPM140	140 μm	0.1 nm

Table 13: Specs of the actuator

It can work in closed loop but then the system becomes more complicated because a real

time measurement has to be done with the required adjustment imposed on the piezoelectric actuator. It can also work in open loop which is easier to implement. A signal of 0V corresponds to a motion of 0 μm, and 10V induces the maximal motion so here 140 μm. So the travel range corresponds to what need to be done to align the mirrors. This piezoelectric actuator has also a very good resolution of 0.1 nm.

It has to be fixed on a stage to provide the linear motion in the right direction to the mirror. An application example is given in Figure 57.

Initially, this product is not made for a vacuum environment but modifications can be done so that it corresponds to the norms. Indeed, NPM series actuators are available as vacuum and cryogenic version.

Finally, the important is to ensure that this kind of device exists and that it is possible to deploy the telescopes and to to adjust them with a nanometer precision.

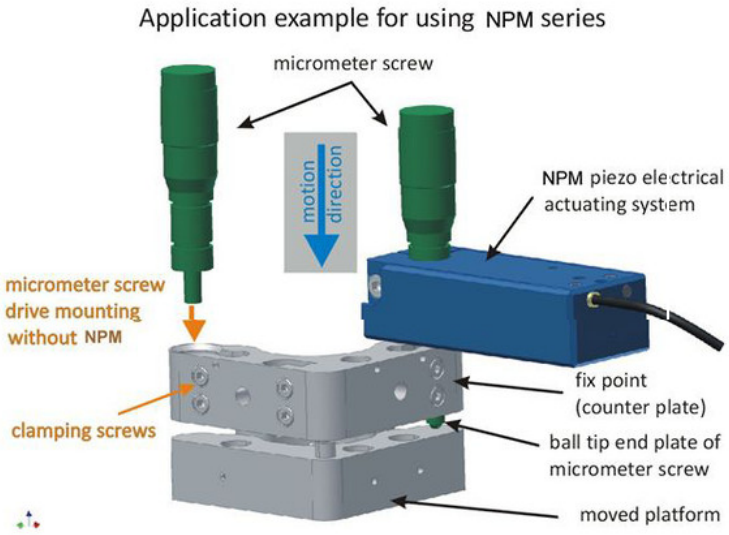

Figure 57: Linear Stage from Newport

6.2 Vibrations compensations

As explained, this device has to be used only once to align the mirrors when the structure is deployed. However, after that the structure might undergo vibrations during the observations due to the spacecraft attitude control. As shown by the modal analysis, the displacements of the CubeSats will mostly happen for accelerations applied in the y and in the z direction. So it is conceivable to use other devices similar to the NPM140 to overcome the signals perturbations.

6.2.1 Acceleration in z direction

For an acceleration of 1g in the z direction, the node A will move in each direction with the values given in Table 14.

	Direction x [mm]	Direction y [mm]	Direction z [mm]
Node A	0.0943	0.0559	1.6675

Table 14: Displacements in all axis for vertical acceleration

Moreover the structure will undergo a rotation in the plane $x - z$ corresponding to the front view of the satellite of 0.0169°and in the plane $y - z$, corresponding to the side view, this rotation is about 0.0284°. As a reminder, the next figure shows the movement of the structure when it is excited with a vertical acceleration at a frequency of 84 Hz.

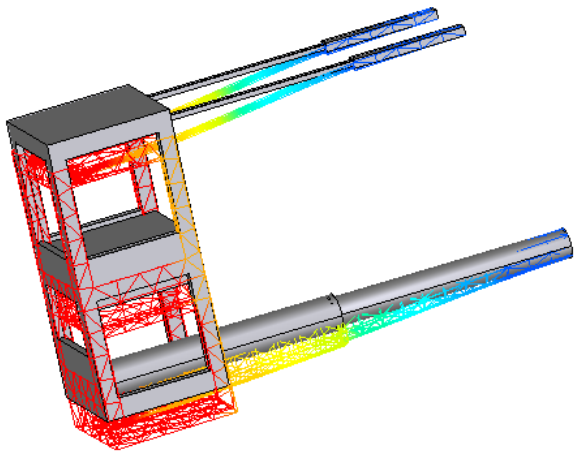

Figure 58: Deformed structure

Thus the displacement happens mainly in the vertical direction, as it could be expected. The guiding rails limit the rotation of the structure to only a few hundredths of a degree. And this can be compensated by a piezoelectric actuator.

6.2.2 Acceleration in y direction

In the same way, here are detailed information about the displacements induced by an acceleration in the y direction. The displacements in each direction are given in Table 15, and as expected the structure moves mainly in the excited direction.

	Dep x [mm]	Dep y [mm]	Dep z [mm]
Node A	0.6267	5.0344	0.4293

Table 15: Displacements in all axis for lateral acceleration

The displacements are more important here but are given for an acceleration of 1g. In practice, the perturbations will most likely never reach that magnitude. Figure 59 illustrates the displacements that correspond here to the first mode shape.

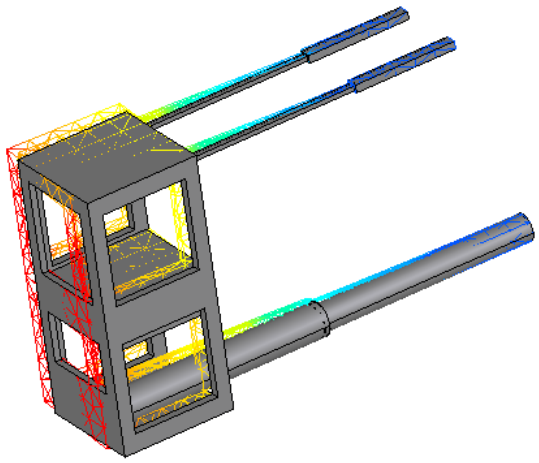

Figure 59: Deformed structure

Finally, two other piezoelectric actuators similar to the NPM140 can be used. So that when the structure is submitted to a disturbance in the y or in the z direction with a frequency close to one of the two first mode shapes, the device can compensate with the same frequency the displacements and keep the good functioning of the telescopes.

6.3 Resolution improvement

As already explained, the angular resolution of a telescope depends on the ratio between the wavelength observed and the diameter of the mirror. This is the reason why two telescopes were placed inside the spacecraft and then deployed. This improved in several manners the resolution.

First the diffraction of mirrors and lens induces a theoretical maximum to the resolution of any optical system. The best obtainable resolution is given by the Rayleigh criterion :

$$\theta = 1.22\frac{\lambda}{D}$$

where θ is the angular resolution in radian, λ is the wavelength observed and D the diameter of the lens aperture. For this work the observations are made in the visible, which gives $\lambda = 550$ nm, the mean value of the visible spectrum, and the diameter of one telescope is $D = 95$ mm. Actually, θ corresponds to the minimum angle that has to separate two points so that they are resolvable.

When the structure is deployed and two telescopes are used D is taken as the distance between the extremities of both telescopes. Here use three tubes for the telescopic boom increases the resolution obtained. The resolutions obtained for all cases are listed in Table 16.

	Single telescope	Deployment - two tubes	Deployment - three tubes
Resolution θ	1.32 arcsec	0.19 arcsec	0.12 arcsec

Table 16: Angular resolutions

These values correspond just the theoretical maximum that could be reached if the mirrors were positioned with a perfect precision. So they do not correspond to the resolution of the deployed telescopes. Nevertheless, they give an idea of the difference between a deployment with two or three tubes, which is not negligible. And they demonstrate that deploy the telescopes divided the theoretical resolution by ten.

However, there are losses of resolution due to the deployment and to the inaccurate positioning of telescopes. Even if they can be compensated by actuators such as the NPM140, it is never possible to reach the theoretical resolution.

Finally another advantage induced by the utilization of two telescopes instead of one is that the flux received by the collecting mirrors is doubled. In the end, even if there are losses due to the mechanical precision of the deployment, use interferometry with two telescopes improves largely the resolution.

7 Final Design

Now that all the subsystems composing the satellite have been defined it is important to ensure that the spacecraft matches the CubeSat 6U requirements. These requirements are mainly the mass that cannot be higher than 12 kg, the geometry which has to respect the dimensions 10 cm x 22.63 cm x 36.6 cm and the position of the center of gravity which has to follow constraints of positioning relative to the geometrical center. Moreover, it is necessary to verify that the power needed for the different subsystems can be provided by the solar panels.

So all these aspects are checked in this section that establishes the critical budgets of the mission.

7.1 Respect of the dimensions

The design of the CubeSat including all the components has already been shown and is visible in Figure 60. As it can be observed, all the elements fit inside the chassis which has the required dimensions. So there is no problem of respect of dimensions.

7.2 Mass computation

Here is detailed the mass of all the components with still two cases differentiated according to the number of tubes composing the telescopic boom. The difference between these cases comes from the booms and the guiding rails which are longer thus heavier, and from the deployer that add 0.037 kg by meter deployed.

Components	Mass [kg]	
	Two Tubes	Three Tubes
Chassis	0.9	
Structure	0.84	
Communications	0.062	
ADCS	1.5	
Mirrors	0.450	
Mirrors inclined at 45°	0.015	
Detector	0.15	
On board Computer	0.094	
EPS	0.054	
Solar Panels	0.3	
Piezoelectric Actuator	0.125	
Deployer	0.189	0.207
Telescopic Tube	0.051	0.077
Guiding rails	0.017	0.025
Total mass	4.747	4.799

Table 17: Mass of the CubeSat

The mass of the mirrors was evaluated to 150 g for a single telescope by Christian Kintziger. The structure corresponds to all the parts added to the chassis and is used mainly to support the different subsystems. Finally, the number of tubes used in the telescopic boom has not a big influence on the total mass. As it can be observed, this total mass is far from

the limitation of 12 kg so even if other components have to be added the mass budget is not a problem.

7.3 Position of the center of gravity

The CubeSat center of gravity shall be located within 4.5 cm from its geometric center in the y direction, within 2 cm from its geometric center in the z direction, and within 7 cm from its geometric center in the x direction, still with the same frame of reference.

So the position of the center of gravity has to be computed, because it has to respect the specifications given by the CubeSat Program in order to ensure the good deployment from the dispenser. For this computation, only the total mass of systems such as ADCS are known and not the exact position of their center of gravity. So for these components the assumption of a uniform density is made, and their center of gravity is taken as their geometrical center.

For the measures, the center of the frame is taken at the point O of Figure 60 which is situated in the middle of the satellite along the x axis so that the center of gravity should be close to zero in that direction. And in the vertical direction the center of gravity of subsystems are measured from the bottom.

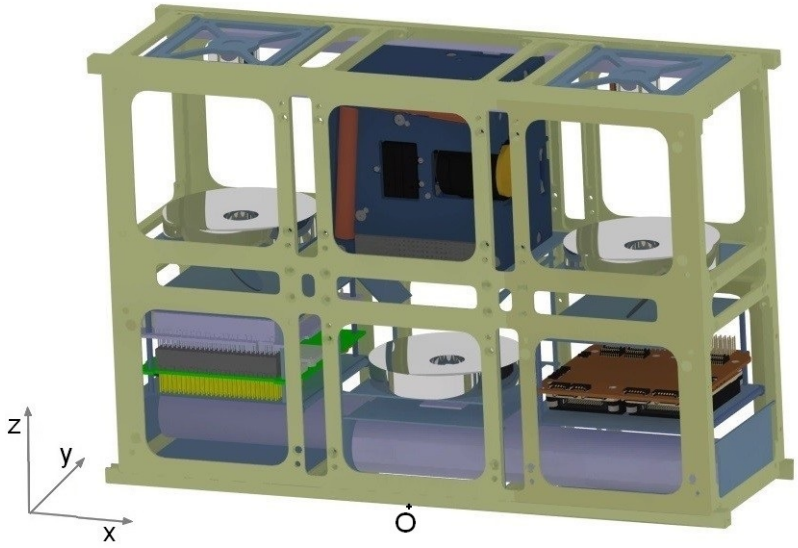

Figure 60: CubeSat in initial configuration

First, in the vertical direction there is no symmetry. So the center of gravity has to be determined for all the components in this direction. Then, the position has to be computed also in the x direction because the two external CubeSats are not symmetrical, the systems they carry are not exactly the same. And eventually, the center of gravity can be directly determined in the y direction because in this direction all the components are symmetric with respect to the center, except the telescopic tubes which are shifted. But they are both shifted from the same distance and so compensate the difference so that the center of gravity corresponds to the geometrical center for this direction.

Components	Direction x [mm]		Direction z [mm]	
Chassis	0		113.15	
Structure	0		95.5	
Communications	-110.35		60.1	
ADCS	0		170.85	
Mirrors	0		126.68	
Mirrors inclined at 45°	0		101.9	
Detector	0		42.3	
On board Computer	-110.35		83.56	
EPS	110.35		56.2	
Solar Panels	0		113.15	
Piezoelectric Actuator	0		112	
Deployer	0		15	
Telescopic Tube	0		21.8	
Guiding rails	0		216.125	
	Two tubes	Three tubes	Two tubes	Three tubes
Total position	-2.371	-2.345	120.79	120.016

Table 18: Center of gravity of the CubeSat

Here, there are no distinctions between the two cases for the position of the different elements. Indeed, in the initial configuration, the elements are placed in the same way whatever the number of tubes. However, they have not the same mass as seen in Table 17, which explains the slight difference in the total position of the center of gravity.

In the longitudinal direction so along the axis x this position is slightly shifted toward one side of the spacecraft, the one that has one component more and that is on the left in Figure 60. And in the vertical direction, the center of gravity is upper than the geometrical center which is placed at 113.15 mm from the bottom. However, it is still largely in the margins imposed by the CubeSat specifications in the three directions. And here again add a third tube to the telescopic booms does not result in a big difference.

7.4 Power consumption

Table 19 lists the power needed by the different systems. Sometimes they are characterized by a nominal value and a peak power, both values are given in the next table.

Components	Power needed [W]
Communications	3.8
ADCS	2 - 4
On board Computer	0.4 - 0.55
Detector	3
Total consumption	9.2 - 11.35

Table 19: power consumption of the CubeSat

So if all the components work in nominal conditions, they require only 9.2 W. And in the worst conditions, the peek power needed is 11.35 W. The solar panels for a CubeSat 6U

can provide up to 17 W, so the piezoelectric actuators cannot use more than 5.65 W to stay under the budget supplied by the solar panels even in the worst conditions.

7.5 Future work

All this work is based on a purely theoretical study of the feasibility of such a mission. To validate the results obtained it is important to carry out different tests. These simulations have to be used to ensure the good functioning of the different mechanisms, particularly the deployment of the CubeSats and the locking of the system is the deployed configuration.

8 Conclusion

This study investigated the feasibility of using interferometry on a CubeSat to improve the resolution of observations. So the objective was to deploy from a single CubeSat telescopes that would collect light and send it toward a central telescope with a detector.

The first part was devoted to a review of the state of the art of deployable structures in spacecrafts and more specifically in small satellites. The different kind of deployment mechanisms were described with their characteristics and information on past missions that used that technology.

Then a preliminary design of the spacecraft was made. Because the satellite had to transport two telescopes, a CubeSat 6U was selected. This design enabled to determine the space dedicated to the deployment system.

From this information it was possible to select the most appropriate deployment mechanism to use. Comparing the characteristics of all the techniques it was decided that the telescopic booms were the best choice.

After that, the functioning of the deployment was discussed in more details. The motorization, the kinematics and the locking mechanism of the telescopic boom were studied and the telescopic tubes were designed.

There, an improvement of the rigidity of the deployed structure was done. Guiding rails based on a passive deployment were added to strengthen the deployed structure. Indeed, they bring several benefits and in particular they prevent the rotation of the structure.

To evaluate the rigidity of the structure a modal analysis was conducted. The ten first mode shapes of the deployed satellite were computed for several cases that compared the differences between a telescopic boom composed of two or three tubes. The influence of the guiding rails was also assessed.

It was concluded that they had a major importance because they allowed to increase the value of the first eigenfrequencies and to separate the two first modes of the structure. Therefore, they permit to decrease the value of the displacements caused by a perturbation, in addition to prevent the rotation.

The response of the spacecraft to external accelerations was also computed. And specifications have been established about the maximal frequency and amplitude permissible for the telescopes.

Then, a short thermal analysis of different cases was carried out to determine the temperature of the CubeSat in different orbit configurations. This permitted to evaluate the induced elongation of the telescopic booms.

The optic part was about the possibilities that could be used to improve the cophasing of signals coming from deployed telescopes. The option to use a piezoelectric actuator to compensate the deployment imprecision was studied. Similarly, the possibility to overcome vibrations due to accelerations was considered. After that, the theoretical resolution of the deployed system was computed.

Finally, a budget evaluation of the entire system was done with a calculation of the mass of the spacecraft as well as an evaluation of its center of gravity and its power consumption. It was assessed that the satellite respected the 6U CubeSat requirements.

Annexes

A First modes shape

Here are represented the ten first mode shape of the structure.

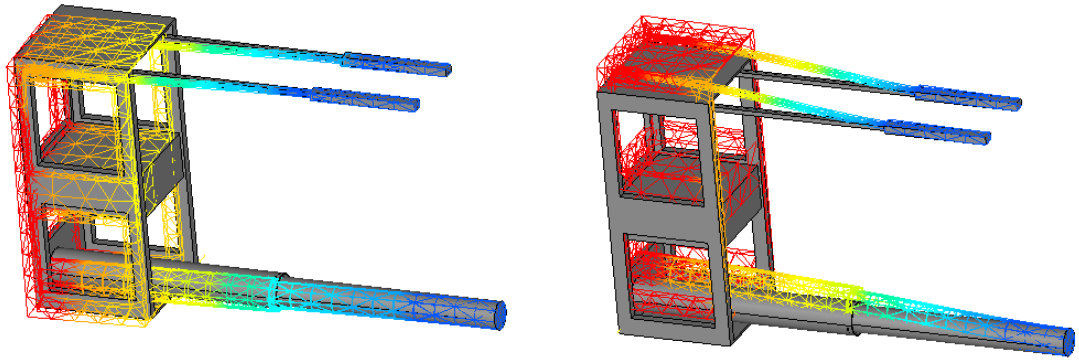

Figure 61: Modes 1 & 2

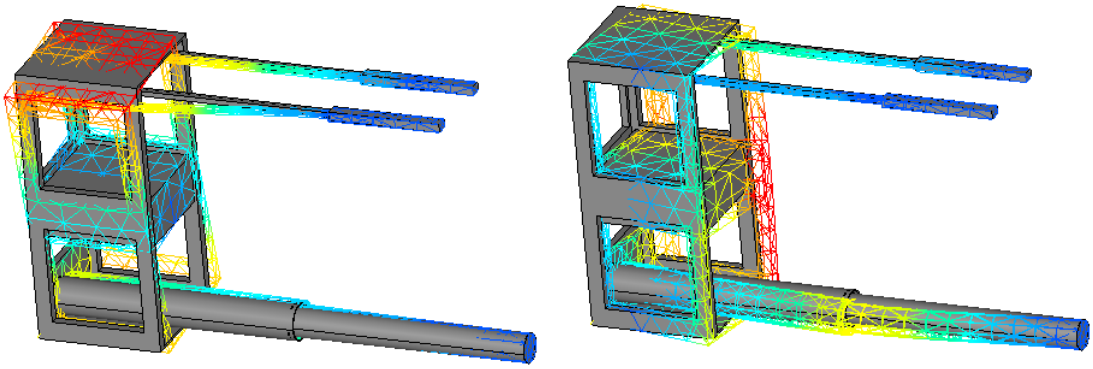

Figure 62: Modes 3 & 4

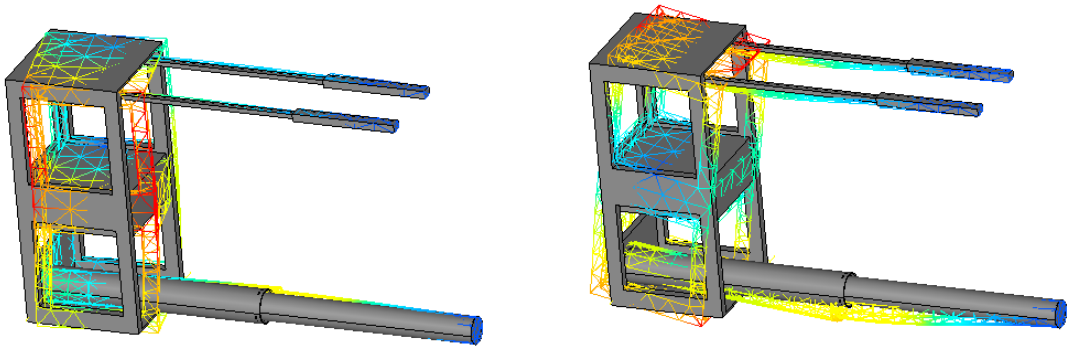

Figure 63: Modes 5 & 6

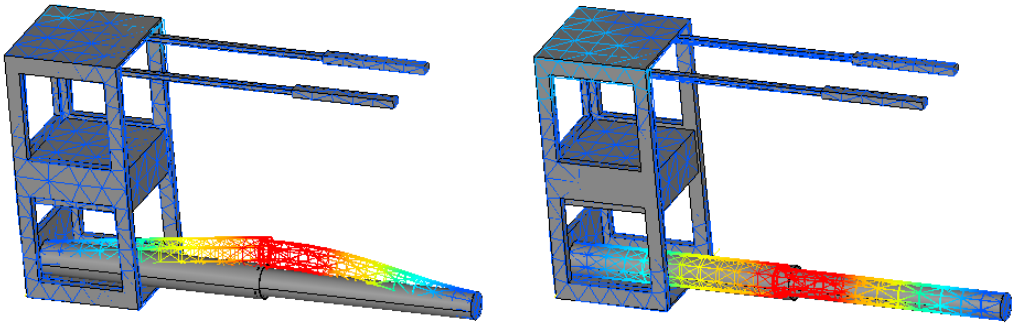

Figure 64: Modes 7 & 8

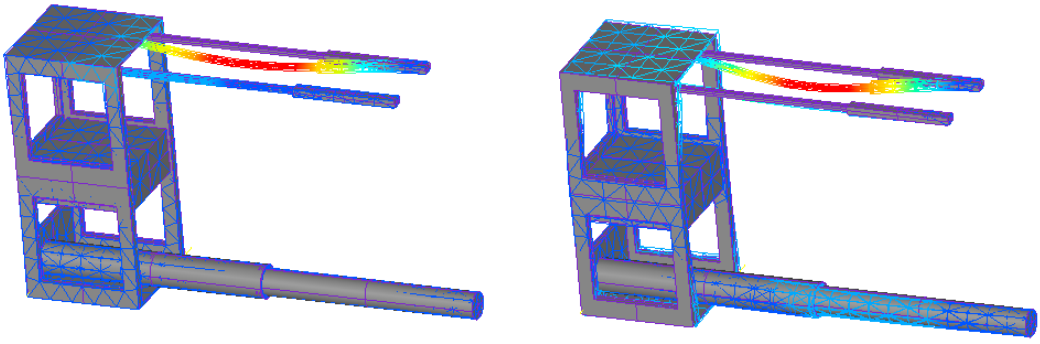

Figure 65: Modes 9 & 10

B View Factor

Here is the formula for the view factor between two parallel rectangles.

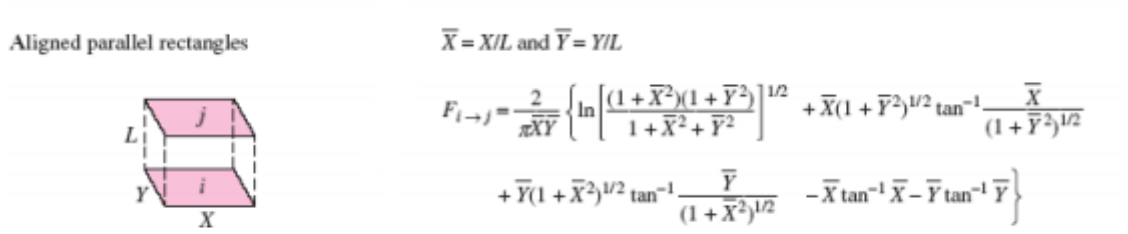

Figure 66: View factor between parallel rectangles

[normalem]ulem

References

[1] California Polytechnic State University. Cubesat design specification rev 13. https://static1.squarespace.com/static/5418c831e4b0fa4ecac1bacd/t/56e9b62337013b6c063a655a/1458157095454/cds_rev13_final2.pdf, 2017. consulted on 2017-05-17.

[2] California Polytechnic State University. Cubesat design specification rev. 13. https://static1.squarespace.com/static/5418c831e4b0fa4ecac1bacd/t/573fa2fee321400346075f01/1463788288448/6U_CDS_2016-05-19_Provisional.pdf, 2017. consulted on 2017-05-08.

[3] Herbert J. Kramer. Cubesat concept. https://directory.eoportal.org/web/eoportal/satellite-missions/c-missions/cubesat-concept#top, 2017. consulted on 2017-04-19.

[4] Erik Kulu. World's largest database of nanosatellites more than 1600 nanosats and cubesats. http://www.nanosats.eu, March 2017. consulted on 2017-05-29.

[5] Herbert J. Kramer. Isara. https://directory.eoportal.org/web/eoportal/satellite-missions/i/isara, 2017. consulted on 2017-04-09.

[6] Gunnar Tibert. Deployable tensegrity structures for space applications. April 2002. PhD thesis, *Royal Institute of Technology*.

[7] Jonathan Sauder, Nacer Chahat, Mark Thomson, Richard Hodges, Eva Peral, and Yahya Rahmat-Samii. Ultra-compact ka-band parabolic deployable antenna for radar and interplanetary cubesats. 2014. *29th Annual AIAA/USU Conference on Small Satellites*.

[8] Noah Schwartz, David Pearson, Stephen Todd, Andy Vick, David Lunney, and Donald MacLeod. A segmented deployable primary mirror fro earth observation from a cubesat platform. 2014. *29th Annual AIAA/USU Conference on Small Satellites*.

[9] Matthew G. McHarg, Brian A. Smith, Timothy H. Russell, Olha Asmolova, Trey S. Quiller, Richard L. Balthazor, Michael E. Dearborn, Brooke M. Isch, Taylor R. Johnson, Angus J. MacDonald, and Eric W. Peek. Falconsat-7 - a deployable solar telescope. 2014. *29th Annual AIAA/USU Conference on Small Satellites*.

[10] Orbital ATK. Coilable boom systems. https://www.orbitalatk.com/space-systems/space-components/deployables/docs/Fact%20Sheet%20-%20Coilable%20Boom%20Systems.pdf, 2017. consulted on 2017-03-22.

[11] Yuya Nakamura, Ryu Funase, Masaki Nagai, Akito Enokuchi, Yuta Nojiri, Tsukasa Funane, Fumiki Sasaki, and Shinichi Nakasuka. Extendible boom-based optical system for nano-scale remote sensing satellite prism. 2005. *19th Annual AIAA/USU conference on small satellites*.

[12] Pau Mallol Parera. Deployment simulations of a composite boom for small satellites. May 2013. *Technical Reports from Royal Institute of Technology, Department of Mechanics, Stockholm*.

[13] Mark Schenk, Andrew D. Viquerat, Keith A. Seffen, and Simon D. Guest. Review of inflatable booms for deployable space structures: Packing and rigidization. Vol. 51(No 3):pp. 762–778, May-June 2014. *Journal of Spacecrafts and Rockets.*

[14] A. Viquerat, Schenk M., B. Sanders, and V. Lappas. Inflatable rigidisable mast for end-of-life deorbiting system. 2014. *Proceedings of the 13th European Conference on spacecraft structures, materials environmental testing : 1-4 April.*

[15] Brian Engberg, Greg Spanjers, Peter Wegner, Daron Bromaghim, CIC Pamela Fetchko, Lt Col Jerry Sellers, Mark Lake, Mike Tupper, Jeff Harvey, and Jon Evans. A high stiffness boom to increase the moment-arm for a propulsive attitude control system on falconsat-3. 2003. *17th Annual AIAA/USU Conference on Small Satellites.*

[16] Oxford Space Systems. Astrotube max telescopic boom. `https://www.oxfordspacesystems.com/`, 2016-2017. consulted on 2017-03-30.

[17] Herbert J. Kramer. Quakesat. `https://directory.eoportal.org/web/eoportal/satellite-missions/q/quakesat`, 2017. consulted on 2017-05-11.

[18] Orbital ATK. Articulated mast systems. `https://www.orbitalatk.com/space-systems/space-components/deployables/docs/FS016_15_OA_Articulated%20Mast%20Systems.pdf`, 2015. consulted on 2017-04-20.

[19] Sierra Nevada Corporation's Space Systems. Space technologies product catalog 2015, rev. 5. page 7, 2015.

[20] Spaceflight 101. Alsat-nano. `http://spaceflight101.com/pslv-c35/alsat-nano/`, 2017-06-10. consulted on 2017-06-10.

[21] Northrop Grumman. Storable tubular extendable member. `http://www.northropgrumman.com/BusinessVentures/AstroAerospace/Products/Pages/STEM.aspx`, 2017. consulted on 2017-03-16.

[22] Peter Fortescue, Graham Swinerd, and John Stark. Spacecrafts systems engineering. 2011. *Wiley.*

[23] Lionel Bourrec, Lauren Barnabe, Victor Pires, and Sylvain Tremolieres. Telescopic boom for space applications engineering model. 2011. *14th European Space Mechanisms & Tribology Symposium - ESMATS.*

[24] Christian Kintziger. Feasibility of a uv imager onboard a cubesat platform. Master's thesis, Université de Liège, 2012-2013.

[25] CubeSat Shop. On board computer. `https://www.cubesatshop.com/product/on-board-computer/`, 2017. consulted on 2017-03-27.

[26] CubeSat Shop. Isis txs s-band transmitter. `https://www.cubesatshop.com/product/isis-txs-s-band-transmitter/`, 2017. consulted on 2017-03-25.

[27] Hyperion Technologies. iadcs400 attitude determination and control system. `http://hyperiontechnologies.nl/wp-content/uploads/2016/08/HT-iADCS400-V1.01_Flyer.pdf`, 2016. consulted on 2017-03-25.

[28] GomSpace. Nanopower p60 system. `https://gomspace.com/Shop/subsystems/power-supplies/nanopower-p60.aspx`, 2017. consulted on 2017-04-04.

[29] ISIS. Solar panels. https://www.cubesatshop.com/wp-content/uploads/2016/06/ISIS-Solar-Panels-Brochure-v1.pdf, 2017. consulted on 2017-05-20.

[30] Pierre Rochus. Space environment & constraints. 2015. *Space experiment development*, Université de Liège.

[31] Pierre Rochus. Space lubricants. 2015. *Space experiment development*, Université de Liège.

[32] M.W. Thomson. Deployable and retractable telescoping tubular structure development. 1994. *28th Aerospace mechanisms symposium.*

[33] Northrop Grumman. Stem products & programs. http://www.northropgrumman.com/BusinessVentures/AstroAerospace/Products/Documents/pageDocs/STEM_Hardware_Programs.pdf, 2017. consulted on 2017-05-12.

[34] Matthew Long, Allen Lorenz, Greg Rodgers, Eric Tapio, Glenn Tran, Keoki Jackson, Robert Twiggs, and Thomas Bleier. A cubesat derived design for a unique academic research mission in earthquake signature detection. 2002. *16th Annual/USU Conference on Small Satellites.*

[35] Adam Thurn, Steve Huynh, Steve Koss, Paul Oppenheimer, Sam Butcher, Jordan Schlater, and Peter Hagan. A nichrome burn wire release mechanism for cubesats, May 16-18, 2012. *Proceedings of the 41st Aerospace Mechanisms Symposium, Jet Propulsion Laboratory.*

[36] Michel Géradin and Daniel J. Rixen. Mechanical vibrations, third edition, 2015. *Wiley.*

[37] Newport. Piezo-electric open-loop micrometer adapter, 140 μm. https://www.newport.com/p/NPM140, 2017. consulted on 2017-06-02.